

$^{12}\text{CO}(J=1-0)$ ON-THE-FLY MAPPING SURVEY OF THE VIRGO CLUSTER SPIRALS.

I. DATA & ATLAS

E. J. Chung^{1,3}, M.-H. Rhee^{2,3}, H. Kim³, Min S. Yun⁴, M. Heyer⁴, and J. S. Young⁴

rigelej@yonsei.ac.kr

ABSTRACT

We have performed an On-The-Fly (OTF) mapping survey of $^{12}\text{CO}(J=1-0)$ emission in 28 Virgo cluster spiral galaxies using the Five College Radio Astronomy Observatory (FCRAO) 14-m telescope. This survey aims to characterize the CO distribution, kinematics, and luminosity of a large sample of galaxies covering the full extents of stellar disks, rather than sampling only the inner disks or the major axis as was done by many previous single dish and interferometric CO surveys. CO emission is detected in 20 galaxies among the 28 Virgo spirals observed. An atlas consisting of global measures, radial measures, and maps, is presented for each detected galaxy. A note summarizing the CO data is also presented along with relevant information from the literature. The CO properties derived from our OTF observations are presented and compared with the results from the FCRAO Extragalactic CO Survey by Young et al. (1995) which utilized position-switching observations along the major axis and a model fitting method. We find that our OTF derived CO properties agree well with the Young et al. results in many cases, but the Young et al. measurements are larger by a factor of 1.4 - 2.4 for seven (out of 18) cases. We will explore further the possible causes for the discrepancy in the analysis paper currently under preparation.

Subject headings: atlases — galaxies: clusters: individual (Virgo) — galaxies: ISM — radio lines: galaxies

¹Dept. of Astronomy, Yonsei University, Seoul 120-749, Korea

²Yonsei University Observatory, Yonsei University, Seoul 120-749, Korea

³Korea Astronomy & Space Science Institute, Daejeon 305-348, Korea

⁴Dept. of Astronomy, University of Massachusetts, 710 North Pleasant Street, Amherst, MA 01003, USA

1. Introduction

The high galaxy density and the proximity make the Virgo cluster a particularly interesting laboratory for a galaxy evolution study. Its dynamical evolution is still in progress, and evidence for significant environmental effects is ubiquitous (e.g., Chung et al. 2007). The nearness of the Virgo cluster makes it possible to observe its member galaxies with excellent spatial resolution ($1'' \sim 90$ pc). It is the first cluster for which significant HI imaging was done (van Gorkom et al. 1984), and various new HI surveys such as ALFALFA (Giovanelli et al. 2007) and VIVA (Chung 2007) have recently been conducted. The Virgo cluster has also been the subject of many recent multi-wavelength surveys, such as in radio continuum by NRAO VLA Sky Survey (NVSS; Condon et al. 1998), in $H\alpha$ (Koopmann & Kenney 2004; Chemin et al. 2006), in UV by FAUST (Brosch et al. 1997) and Galaxy Evolution Explorer (GALEX) (e.g., Dale et al. 2007), and in IR by Spitzer (Kenney et al. 2008). High quality optical images are also available from the Hubble Space Telescope (HST)/ACS Virgo Cluster Survey (Cote et al. 2004) and Sloan Digital Sky Survey (SDSS).

Here, we present the results from a new imaging survey of $J = 1 \rightarrow 0$ ^{12}CO emission in a large sample of Virgo galaxies in order to address the distribution and characteristics of dense molecular gas in these galaxies. It is well established that molecular clouds are the sites of ongoing star formation (Larson (2003) and references therein), and carbon monoxide (CO) is the most commonly used tracer of molecular hydrogen (H_2), which is the most abundant but invisible component of cold and dense clouds (e.g., Solomon & Barrett 1991). The global H_2 content and its distribution in galaxies and a comparison with other gas and stellar components as a function of morphological type, luminosity, and environment are some of the key insights one can derive from CO observations (see Young & Scoville (1991) and references therein).

Existing CO surveys of Virgo cluster galaxies suffer from limited spatial coverage and small sample sizes. The FCRAO extragalactic survey (Young et al. 1995) is the first CO survey covering a wide range of distance, diameter, morphological type, and blue luminosity of some 300 galaxies conducted using the FCRAO 14-m telescope, including CO measurements (detections and upper limits) of 65 Virgo galaxies. Because of the large observing time required, these observations were conducted in the position-switching mode, primarily along the optical major axis of the disks, and the global CO line luminosity was derived assuming a model distribution. More recently, high angular resolution CO images have been obtained using interferometric measurements by Sakamoto et al. (1999) and Sofue et al. (2003). These measurements reveal a detailed molecular gas distribution at 100 pc scales, but they are limited only to the central region of galaxies. The BIMA SONG (Survey Of Nearby Galaxies;

Helfer et al. (2003)) has also carried out an imaging survey of CO emission in several Virgo spiral galaxies, incorporating the short spacing data from the NRAO 12-m telescope. The total number of Virgo galaxies imaged by the BIMA SONG is small (six), however.

These earlier CO observations have revealed important insights on the molecular interstellar medium (ISM) in these galaxies. For example, CO emission is often centrally concentrated, in contrast to the centrally deficient HI distributions commonly found in these galaxies. The molecular gas distribution also shows little evidence for any influence of the gas stripping mechanisms (e.g., Kenney & Young 1989). No central CO peak (Helfer et al. 2003) or nuclear molecular rings (e.g., Iono et al. 2005) are seen in other cases. The influence of cluster environment on the molecular content is still poorly understood (e.g., Boselli & Gavazzi 2006).

A distinguishing characteristic of our new CO survey is the complete imaging of ^{12}CO ($J=1-0$) emission of a large sample (28 galaxies) of Virgo spirals using the On-The-Fly (OTF) mapping mode of the Five College Radio Astronomy Observatory (FCRAO) 14-m telescope. Our map size of $10' \times 10'$ is larger than the optical diameter D_{25} and it covers the entire stellar disk of each galaxy. The $45''$ angular resolution of the new CO images is well matched to the existing VLA HI data and is well suited for comparison with other high resolution multi-wavelength data. The specific questions we aim to address are :

- 1) To what extent is the CO distribution governed by the disk dynamics?
- 2) Is there a clear phase transition between HI and H_2 as a function of the interstellar radiation field?
- 3) Are there any systematic differences in the CO properties of spiral galaxies in different environments?

We present in this paper the data and the CO atlas from our OTF mapping survey. In section 2, we describe the sample selection. Observations and data reduction process are described in Section 3. The CO atlas and CO properties are presented in Section 4, and our results are compared with those of Young et al. (1995). Molecular gas distribution in individual galaxies is discussed in Section 5, and the summary and conclusion are given in Section 6. The analysis and interpretation of the data addressing the above questions will be presented in our subsequent papers.

2. THE SAMPLE

We initially selected the 42 Virgo spiral galaxies in the magnitude limited sample studied by Kenney & Young (1988). The primary goal of our project is investigating the spatially resolved distribution of molecular gas and their relation to other tracers of activities among the Virgo spirals, and a large angular size is an important consideration. We also considered the total CO flux to increase the detection rate. Given the observing time limitations, a subset of 28 galaxies was observed in the order of CO strength ($S_{\text{CO}} \geq 200 \text{ Jy km s}^{-1}$) and included in this study. The observed galaxies have an optical diameter of 3-10 arcminutes and span a wide range of morphology (Sa to Sc), surface brightness ($9 \lesssim B_{\text{T}}^0 \lesssim 12$), and dust mass ($10^6 \lesssim M_{\text{dust}} \lesssim 10^7 M_{\odot}$). The basic properties of the observed galaxies are summarized in Table 1 and are illustrated in Figure 1. ¹

¹The E-SO galaxy NGC 4649 is included in our sample because it is a companion of a late type spiral NGC 4647.

Table 1. General Properties of the Sample

Galaxy	R.A.	Dec.	Type		R_{M87}	D_{25}	B_T^0	T_{dust}	i	V_{hel}
(1)	(h m s.s)	(d m s.s)	RSA	LEDA	($^{\circ}$)	(arcmin)	(mag)	(K)	($^{\circ}$)	(km s $^{-1}$)
	(2)	(3)	(4)	(5)	(6)	(7)	(8)	(9)	(10)	(11)
N4192	12 13 48.28	14 54 01.2	SbII	2.5	4.8	9.77	10.05	32.7	78	-142
N4212	12 15 39.37	13 54 05.7	Sc(s)II-III	4.9	4.0	3.09	11.37	35.3	54	-82
N4216	12 15 54.39	13 08 58.3	Sb(s)	3.0	3.7	7.94	9.96	29.1	90	131
N4254	12 18 49.56	14 24 59.4	Sc(s)I.3	5.2	3.3	5.37	10.14	34.9	29	2410
N4293	12 21 12.83	18 22 57.6	Sa pec	0.3	6.4	5.50	10.91	35.4	67	930
N4298	12 21 32.75	14 36 22.9	Sc(s)III	5.2	3.2	2.95	11.46	29.7	59	1140
N4302	12 21 42.41	14 35 52.0	Sc(on edge)	5.4	3.1	4.90	11.05	29.7	90	1118
N4303	12 21 54.89	04 28 25.1	Sc(s)I.2	4.0	8.2	6.17	10.04	36.3	19	1570
N4321	12 22 54.89	15 49 20.7	Sc(s)I	4.0	3.9	7.59	9.79	33.5	38	1579
N4402	12 26 07.70	13 06 48.0	Sc(on edge)	3.3	1.4	3.55	11.75	30.5	80	0
N4419	12 26 56.45	15 02 50.2	Sa	1.1	2.8	3.31	11.52	36.1	82	-254
N4438	12 27 45.59	13 00 31.8	Sb(tides)	0.7	1.0	8.71	10.52	32.1	87	80
N4450	12 28 29.49	17 05 06.0	Sab pec	2.3	4.7	5.13	10.61	28.8	43	1958
N4501	12 31 59.16	14 25 13.6	Sbc(s)II	3.4	2.1	6.76	9.67	31.5	60	2280
N4527	12 34 08.50	02 39 10.0	Sb(s)II	4.0	9.8	5.89	10.62	38.3	75	1732
N4535	12 34 20.32	08 11 53.8	SBC(s)I.3	5.0	4.3	6.92	10.35	34.2	41	1958
N4536	12 34 26.93	02 11 18.2	Sc(s)I	4.2	10.2	7.08	10.32	43.9	59	1807

Table 1—Continued

Galaxy	R.A.		Dec.		Type		R_{M87}	D_{25}	B_T^0	T_{dust}	i	V_{hel}
	(h m s.s)	(d m s.s)	RSA	LEDA	($^\circ$)	(arcmin)						
(1)	(2)	(3)	(4)	(5)	(6)	(7)	(8)	(9)	(10)	(11)		
N4548	12 35 26.42	14 29 46.9	SBb(rs)I–II	3.1	2.4	5.25	10.66	27.8	35	486		
N4567	12 36 32.71	11 15 28.4	Sc(s)II–III	4.0	1.8	2.75	11.75	32.6	43	2265		
N4568	12 36 34.30	11 14 17.0	Sc(s)III	4.1	1.8	4.37	10.95	32.6	65	2255		
N4569	12 36 49.80	13 09 46.3	Sab(s)I–II	2.4	1.7	10.47	9.59	34.6	69	-233		
N4579	12 37 43.40	11 49 25.5	Sab(s)II	2.8	1.8	5.62	10.24	30.7	39	1518		
N4647	12 43 32.31	11 34 54.7	Sc(rs)III	5.2	3.2	2.82	11.67	32.0	34	1415		
N4649	12 43 39.66	11 33 09.4	SO ₁ (2)	-4.0	3.2	7.24	9.69		49	1139		
N4651	12 43 42.62	16 23 36.0	Sc(r)I–II	5.2	5.1	3.98	11.01	33.4	50	804		
N4654	12 43 56.57	13 07 35.9	SBC(rs)II	5.9	3.3	5.01	10.56	33.4	58	1034		
N4689	12 47 45.60	13 45 46.0	Sc(s)II.3	4.7	4.3	4.57	11.33	30.5	39	1613		
N4710	12 49 38.90	15 09 56.7	SO ₃ (9)	-0.8	5.3	4.90	11.72	34.9	90	1325		

Note. — The columns are as follows.

Col. (1) — NGC number

Col. (2) & (3) — Right Ascension and Declination at epoch J2000

- Col. (4) — Morphological Type (RSA : Revised Shapley-Ames Catalog)
- Col. (5) — Numerical Morphological Type code from LEDA (Lyon/Meudon Extragalactic Database <http://leda.univ-lyon1.fr>)
- Col. (6) — Angular distance from M87 ($\alpha = 12\text{h}30\text{m}49.18\text{s}$, $\delta = 12\text{d}23\text{m}28.9\text{s}$)
- Col. (7) — Major axis diameter at 25th mag arcsec⁻² in the *B*-band (LEDA)
- Col. (8) — Total *B*-band magnitude corrected for galactic extinction, internal extinction, and k-correction (LEDA)
- Col. (9) — Dust temperature from Young et al. (1989)
- Col. (10) — Inclination (LEDA)
- Col. (11) — Mean heliocentric radial velocity (LEDA)

3. OBSERVATIONS & DATA REDUCTION

3.1. Observations

We carried out On-The-Fly (OTF) mapping observations of CO emission in 28 Virgo galaxies over several observing sessions between January 2002 and February 2003 using the SEQUOIA (SEcond QUabbin Optical Imaging Array) focal plane array receiver on the FCRAO 14-m telescope. The SEQUOIA consists of 16 horns, each with 45'' beam size, configured in a 4×4 array. The backend system used is the Quabbin Extragalactic Filterbanks (QEF), which consists of sixteen independent spectrometers each with 64 channels at 5 MHz resolution, resulting in a total bandwidth of 320 MHz ($\Delta V \sim 830 \text{ km s}^{-1}$). These spectra are calibrated using the standard chopper-wheel method which corrects for atmospheric and ambient temperature losses to yield the corrected antenna temperature T_A^* .

In the OTF mapping mode, the telescope moves fast and smoothly across the target field taking the data continuously, and each map pixel is sampled independently by all 16 independent detector pixels. Therefore, the use of the OTF observing mode offers a significantly improved calibration, relative pointing accuracy and registration, and a much higher dynamic range over the traditional pixel-by-pixel mapping mode. Our OTF observations have fully covered the entire stellar disk of each galaxy multiple times. Typically a 10' × 10' size box centered on each galaxy is mapped with a scan speed of 45'' per second, and the data is stored in every 0.25 second. A reference spectrum is obtained after every or every other row of scan at a location 30' away in the azimuth direction. A 6' × 4' region is mapped for NGC 4536 because of a telescope problem during the observations. NGC 4567 and NGC 4568 is an interacting pair observed simultaneously using a single scanning box, and one data-cube contains both galaxies.

The pointing and focus of the telescope are measured at 2-4 hour intervals by observing the 86 GHz SiO maser in R-Leo. The measured rms pointing error is $\sim 3''$ in both azimuth and elevation, or $\sim 5''$ total.

3.2. Data Reduction

The data reduction is carried out in two steps, initially using the revised-OTFTOOL (Chung et al. 2006) and later the GIPSY² (Groningen Image Processing SYstem; van der Hulst et al. (1992)) package. The revised-OTFTOOL reads in the raw OTF data and produces a map

²<http://astro.rug.nl/~gipsy>

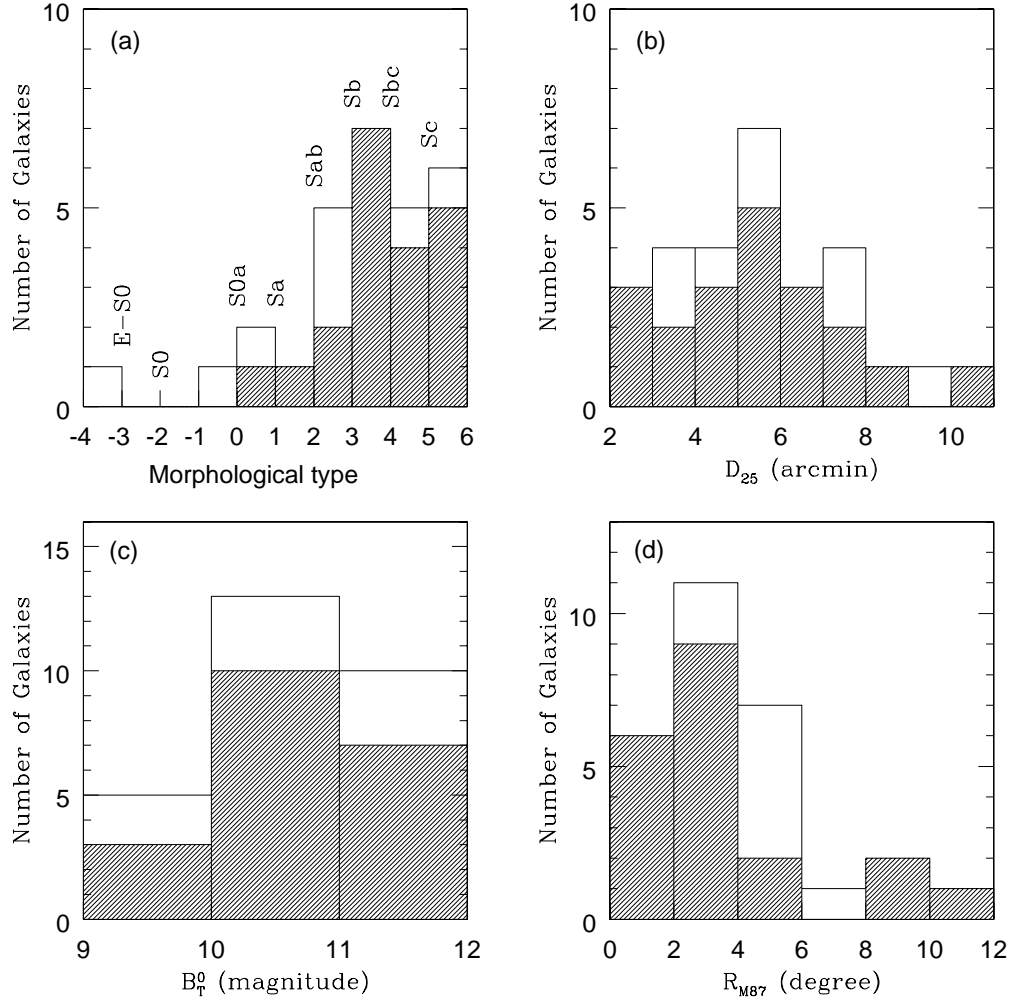


Fig. 1.— The sample properties as a function of (a) morphological type (LEDA), (b) major axis diameter at 25th mag arcsec⁻² in the *B*-band (LEDA), (c) corrected total *B*-band magnitude (LEDA), and (d) angular distance from M87. The white region represents the 28 Virgo galaxies observed, and the shaded region corresponds to the 20 galaxies that are detected in CO.

after the initial editing and calibration. The resulting data cubes are written out in FITS format and are imported to the GIPSY environment for further data reduction and analysis.

The revised-OTF TOOL is a newly developed program based on the OTF TOOL, which is the FCRAO facility pipeline software for the SEQUOIA OTF data. The OTF TOOL was designed primarily for the reduction of narrow Galactic emission line data taken with the digital backend, and the default data filter is not well suited for the baseline removal in the presence of weak, broad emission lines seen in extragalactic CO data. The revised-OTF TOOL includes several new functions that are specifically designed to produce noise-limited output images, with improved data filtering and baseline fitting. An improved filtering algorithm in the revised-OTF TOOL identifies and removes bad spectra using the rms level, antenna trajectory, elevation, and system temperature/gain (T_{sys}), and data containing spikes are identified and excluded. A second major improvement is the implementation of a new self-referencing method. Rather than using the conventional “OFF” spectrum, our self-referencing method constructs the best OFF spectrum from the OTF data itself by choosing the line-free regions in the spatial and spectral domain (see Chung et al. 2005a & 2005b for more detail). This self-referencing method produces an OFF spectrum temporally much closer to the ON spectra, significantly reducing the influence of any residual gain changes and thus a significantly improved baseline behavior. Finally, the data are normally weighted and mapped onto a regular 15” grid.

The GIPSY package is used to produce the final data cubes from the individual scan maps. Occasional bad filter bank channels are removed and replaced with new data generated by interpolating two or more adjacent channels. Interpolation should produce a reasonable result since the channel separation ($\Delta V \sim 13 \text{ km s}^{-1}$) is small compared with the intrinsic CO line width in these galaxies. Data cubes including only the CO emission, used for further spectral analysis, are created in two steps. First, a data mask for the CO emission region is created through an iterative algorithm that identifies the signal regions with criteria of 1.5 rms and minimizes the noise in the line-free regions through a removal of a low-order ($n \leq 2$) polynomial baseline in the frequency domain. Then the final “signal-only” data cube is obtained from the noise-minimized data cube by excluding the noise part and retaining the emission regions. For 6 galaxies which have large inclination ($\gtrsim 80$ degree) or weak emission (S/N ratio $\lesssim 2.5$), Position-velocity diagram (PVD) is used to obtain physical quantities.

Table 2. Information of CO Atlas

Galaxy	CO Intensity map		Velocity field map		PVD ^a		Channel map	
	I_{low} (K km s ⁻¹)	ΔI	V_{sys} (km s ⁻¹)	ΔV	I_{low} (K)	ΔI	I_{low} (K)	ΔI
Group I - Figure 2–14								
NGC 4254	0.230	0.230	2392	20	0.020	0.023	0.024	0.024
NGC 4302	0.096	0.096	1147	40	0.012	0.010	0.016	0.016
NGC 4303	0.160	0.160	1566	20	0.024	0.024	0.024	0.024
NGC 4321	0.210	0.210	1580	20	0.020	0.020	0.020	0.020
NGC 4501	0.160	0.220	2276	40	0.020	0.020	0.024	0.024
NGC 4527	0.240	0.210	1736	40	0.020	0.018	0.021	0.021
NGC 4535	0.220	0.200	1960	20	0.020	0.020	0.030	0.030
NGC 4536	0.140	0.140	1802	20	0.012	0.012	0.012	0.012
NGC 4567*	0.180	0.280	2242	30	0.018	0.018	0.024	0.024
NGC 4569	0.200	0.200	-219	40	0.020	0.020	0.028	0.028
NGC 4647	0.120	0.120	1426	20	0.016	0.016	0.021	0.021
NGC 4654	0.140	0.140	1039	20	0.020	0.020	0.018	0.018
NGC 4689	0.120	0.120	1621	20	0.020	0.020	0.023	0.023
Group II** - Figure 15–17								
NGC 4298					0.012	0.024		
NGC 4402					0.022	0.033		
NGC 4419					0.016	0.024		
NGC 4438					0.018	0.036		
NGC 4548					0.015	0.030		
NGC 4579					0.014	0.021		

Note. — ^a Position-velocity diagram (PVD) of Group I galaxy is shown the central slice of the dataset along the major axis, and that of Group II galaxy is the integrated PVD. The integration is done over some minor axis length for each galaxy (1 or 2 beam-width for highly

inclined galaxies and up to 7 beam-width for weak CO and face-on galaxies).

* NGC 4567 and NGC 4568 are shown in the same map.

** Group II galaxies have weak CO emission and do not show much emission in the channel maps. Therefore only an integrated PVD is shown.

4. RESULTS

Among the 28 galaxies observed, 20 galaxies including a galaxy pair of NGC 4567 and NGC 4568 are detected in CO emission. The CO detected galaxies are classified into two groups : (a) 14 galaxies with strong emission features in the channel map with S/N ratio $\gtrsim 2.5$ (Group I); and (b) 6 galaxies with large inclination $\gtrsim 80$ degree or weak CO emission with S/N ratio $\lesssim 2.5$ (Group II). We have produced a CO atlas for these galaxies and derived their CO properties. NGC 4567 and NGC 4568 are an interacting pair, poorly resolved by our spatial and velocity resolutions. Therefore, their measured and derived properties are reported as a single object. The results of NGC 4536 are derived from $6' \times 4'$ size data cube.

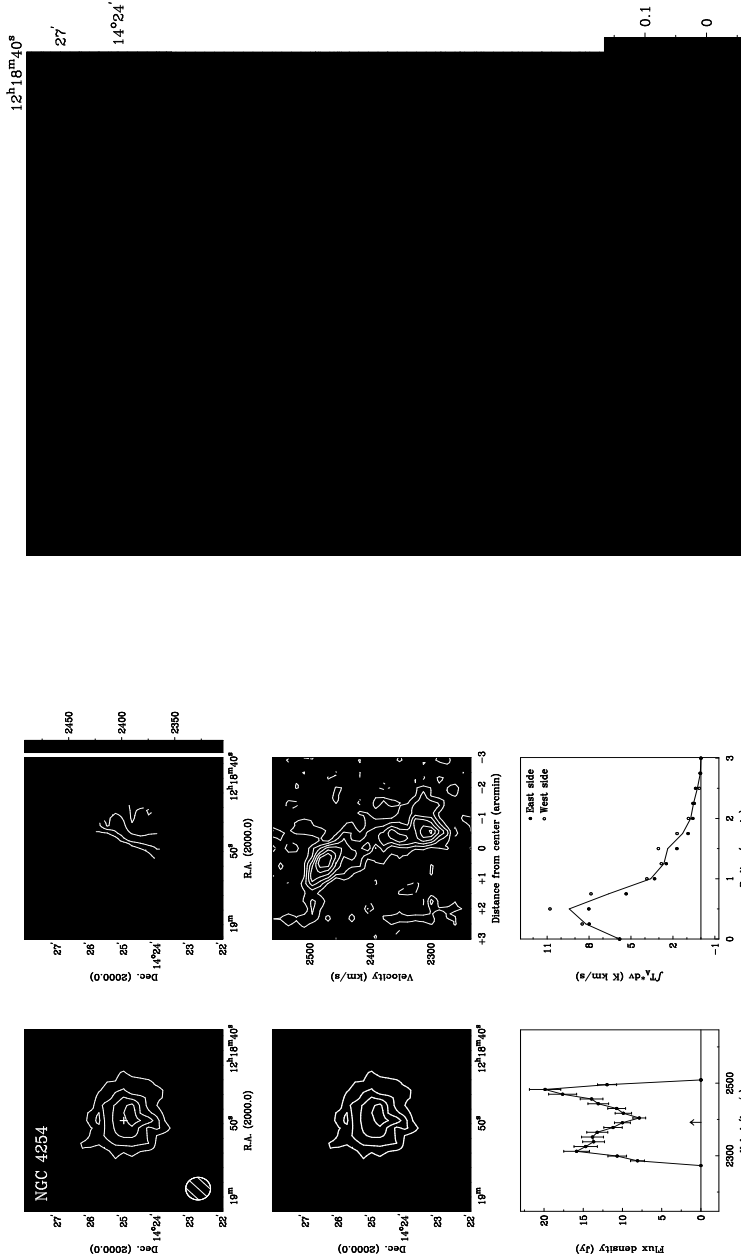


Fig. 2.— Group I-1. CO atlas and channel maps of NGC 4254. CO intensity map (top left), velocity field map (top right), CO contours overlapped on the optical B -band image (middle left), position-velocity diagram which is the central slice along the major axis of data cube (middle right), global CO line profile (bottom left), and radial CO distribution (bottom right). The line of radial profile is the average of the east and west-side values for each radial position. The channel maps are shown over the velocity range of emission. The numbers on top right of the first and second channels represent the velocities in km s^{-1} , and their difference is the channel velocity separation.

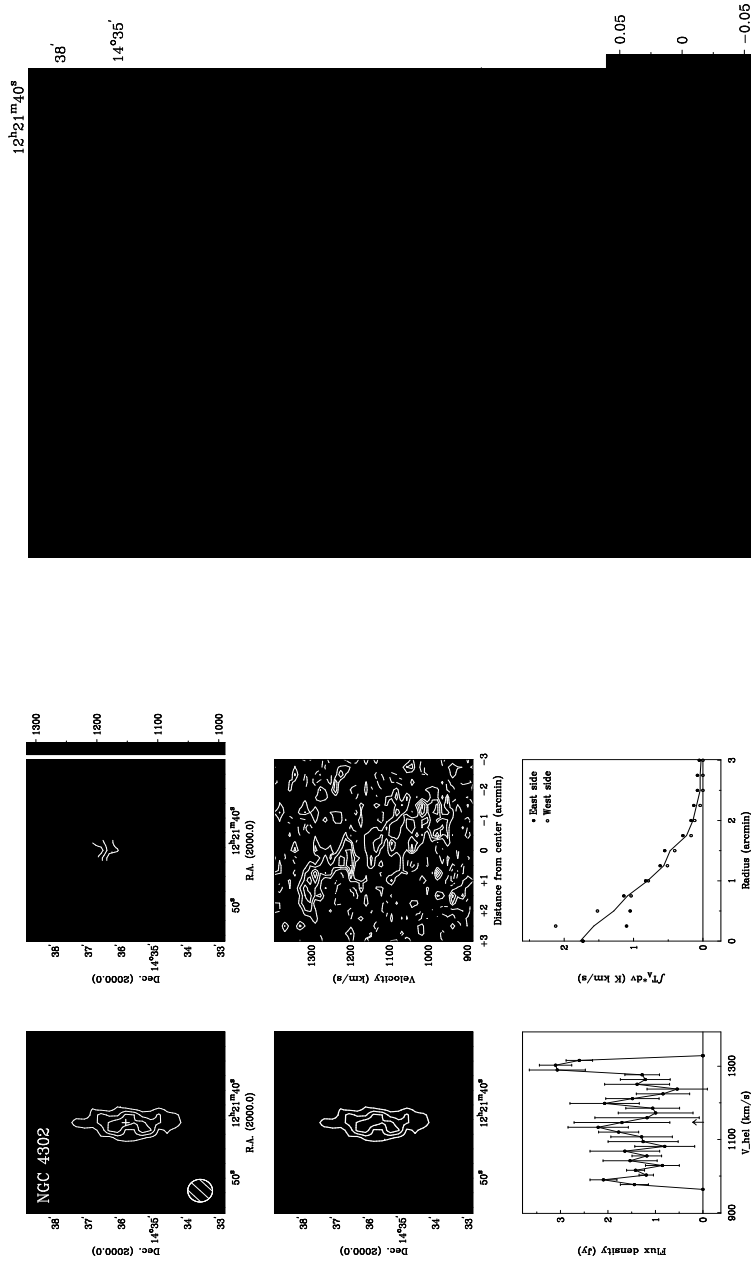


Fig. 3.— Group I-2. Same as Figure 2 for NGC 4302. In the optical image, the companion galaxy NGC 4298 is visible in the east.

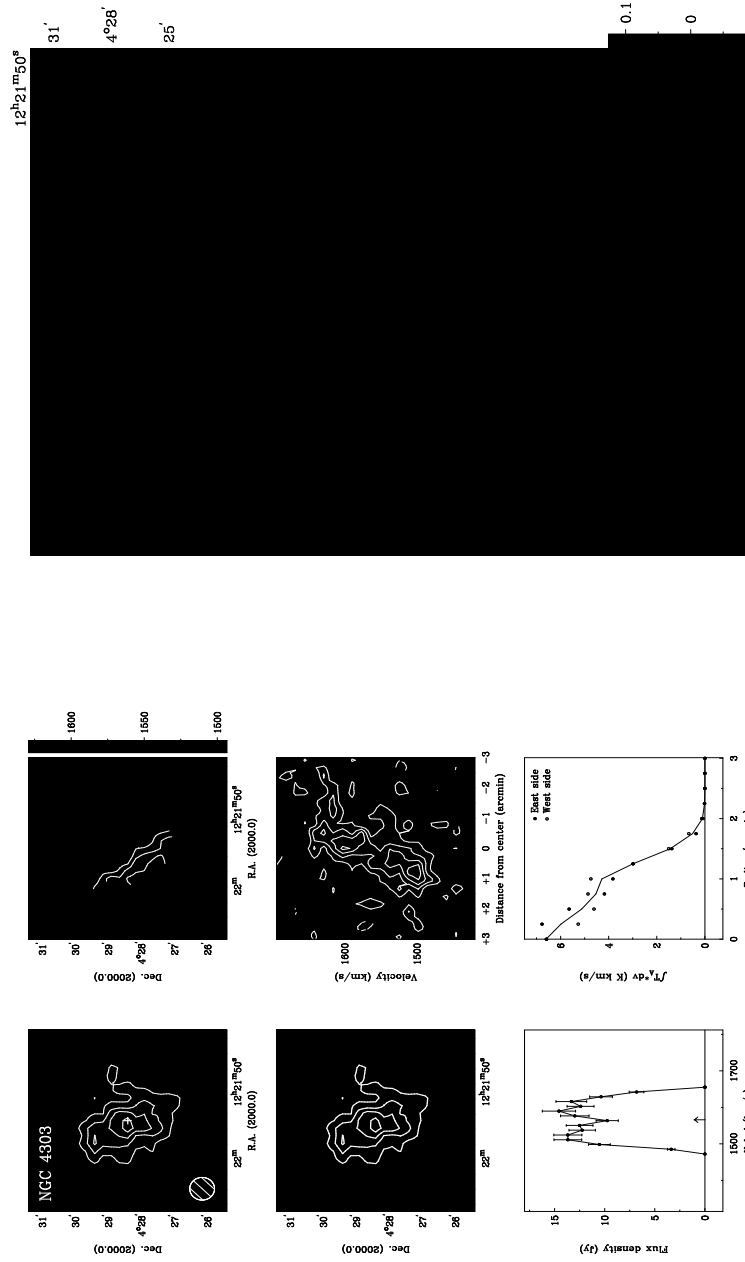


Fig. 4.— Group I-3. Same as Figure 2 for NGC 4303.

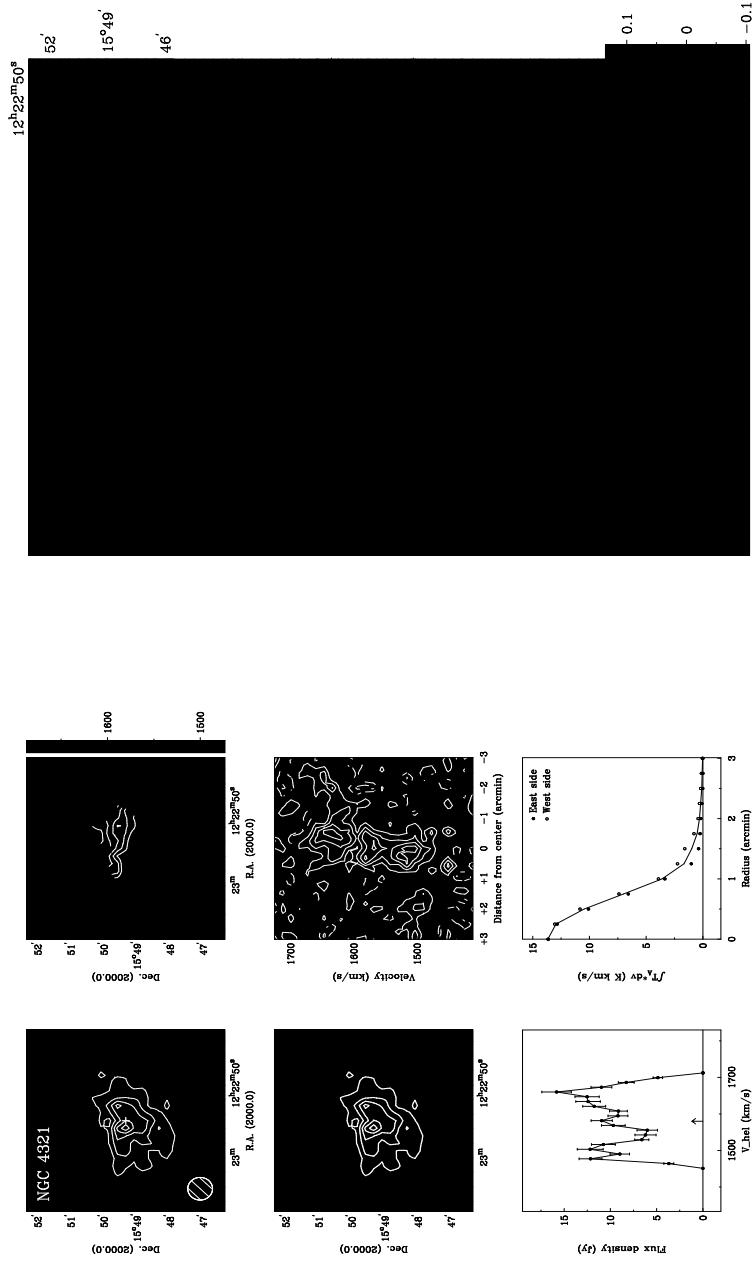


Fig. 5.— Group I-4. Same as Figure 2 for NGC 4321.

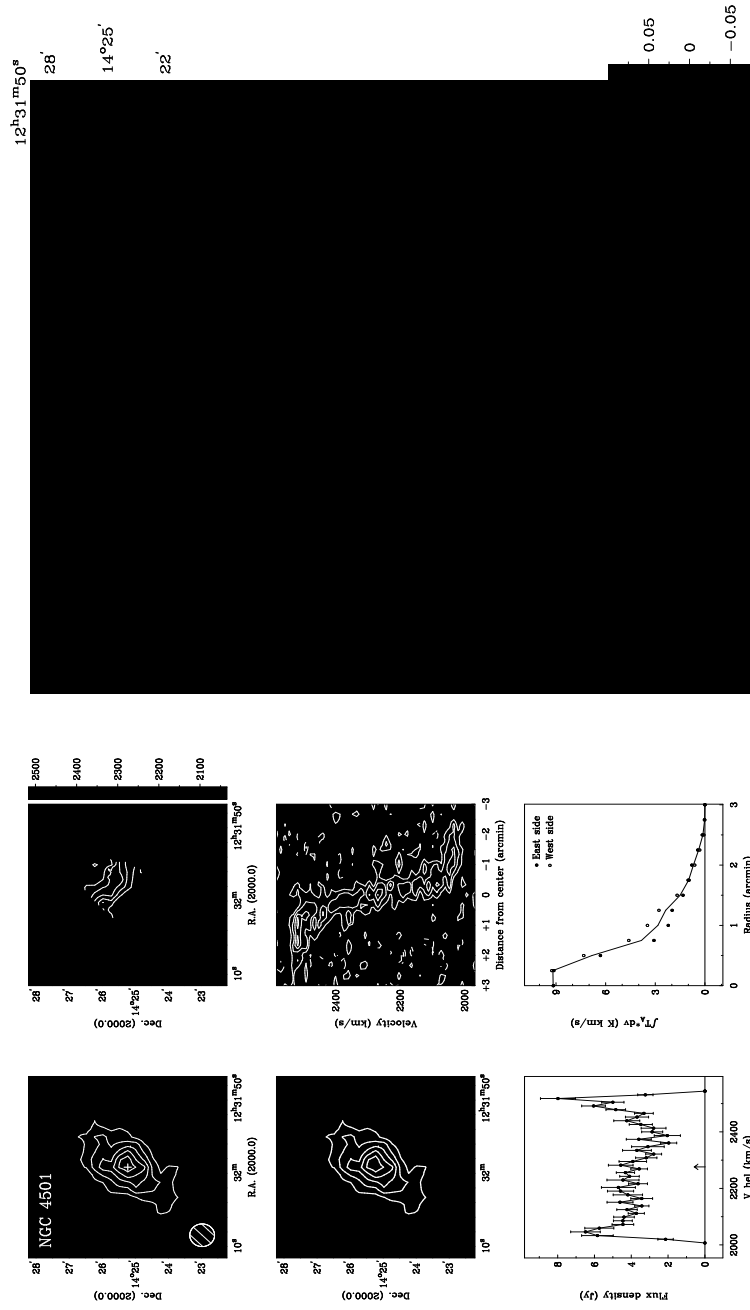


Fig. 6.— Group I-5. Same as Figure 2 for NGC 4501.

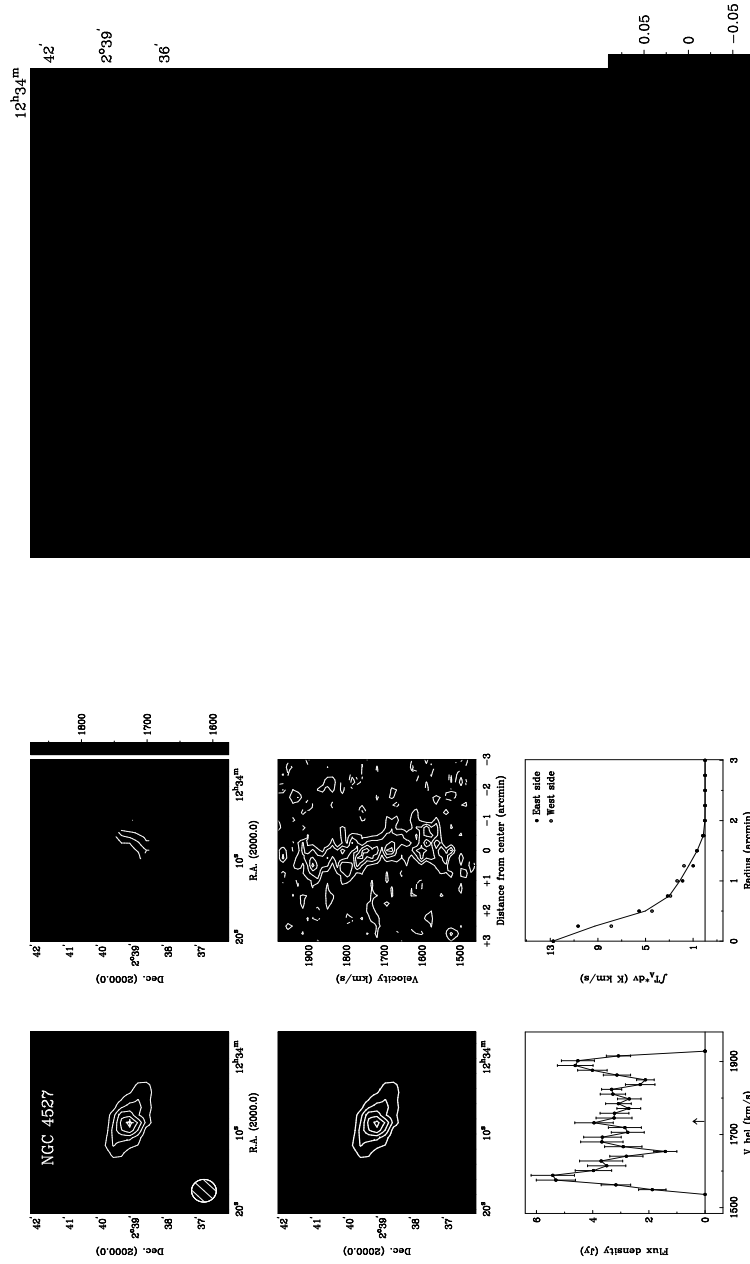


Fig. 7.— Group I-6. Same as Figure 2 for NGC 4527.

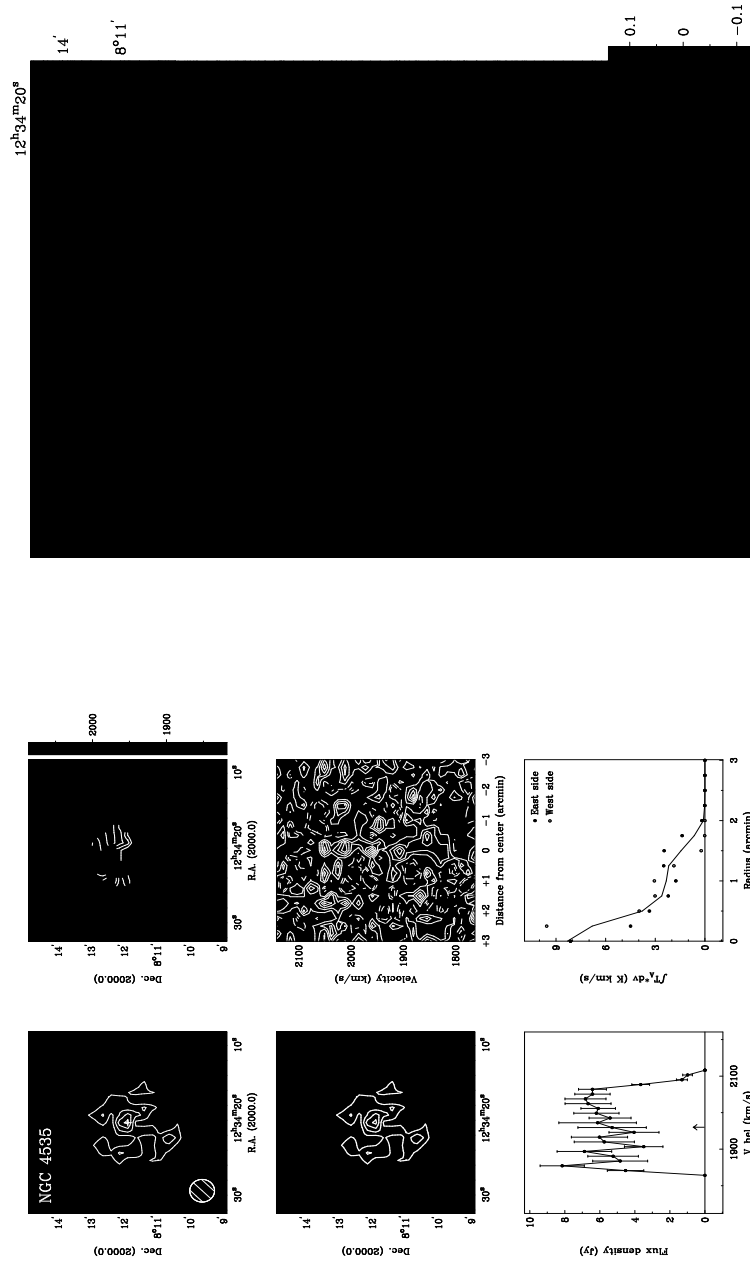


Fig. 8.— Group I-7. Same as Figure 2 for NGC 4535.

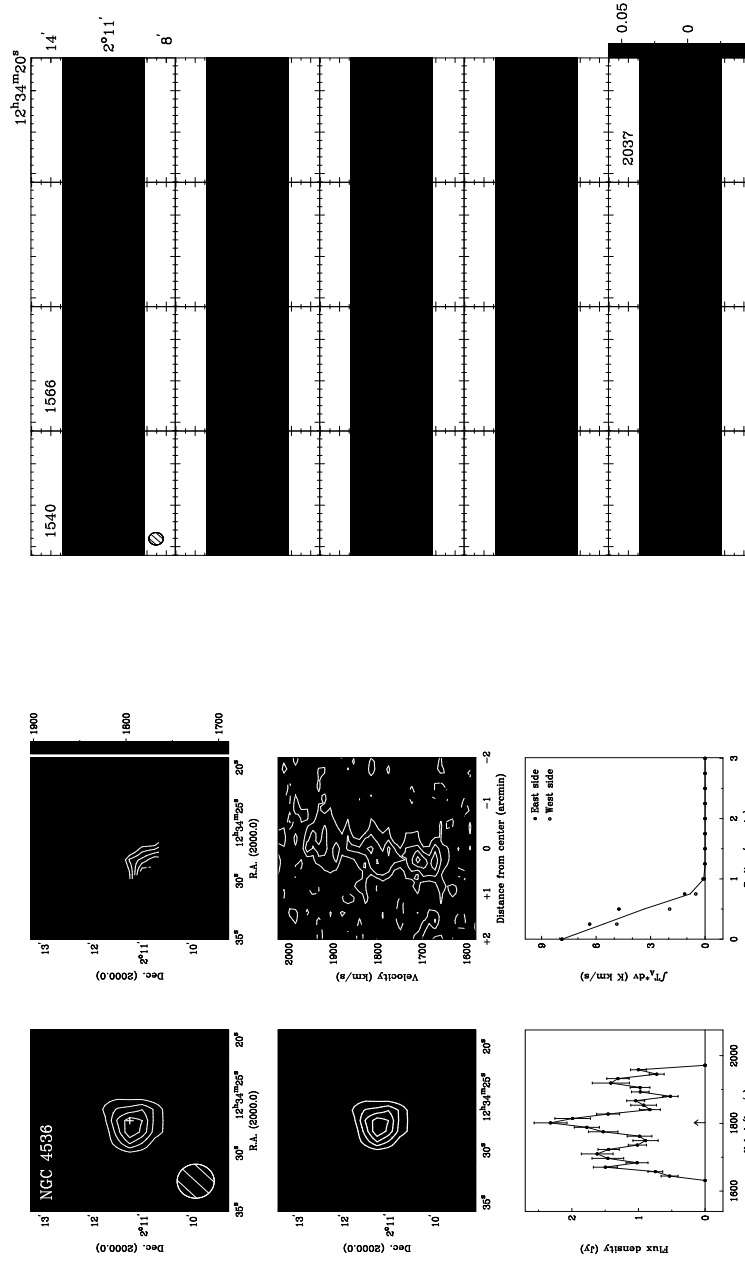


Fig. 9.— Group I-8. Same as Figure 2 for NGC 4536.

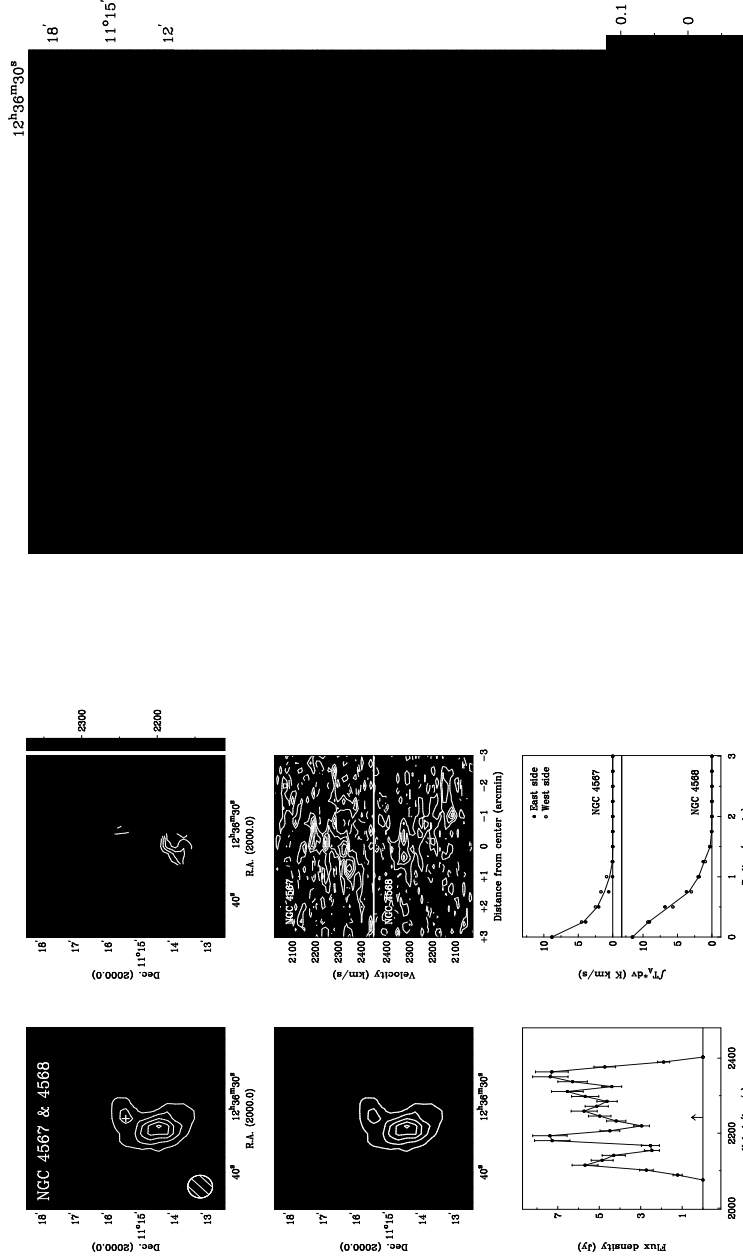


Fig. 10.— Group I-9. Same as Figure 2 for NGC 4567 & NGC 4568. NGC 4567 is in the center, and NGC 4568 is in the south. The PVDs and radial CO distributions are obtained according to each galaxy’s center and position angle.

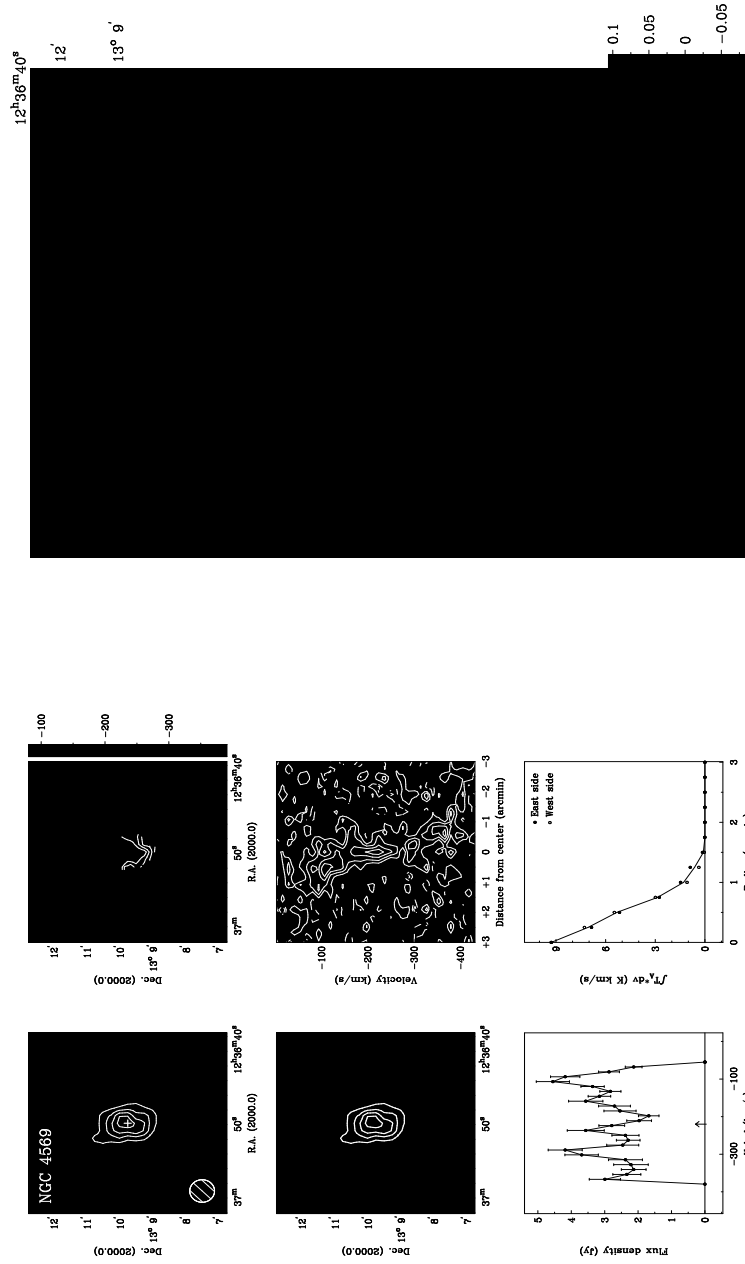


Fig. 11.— Group I-10. Same as Figure 2 for NGC 4569.

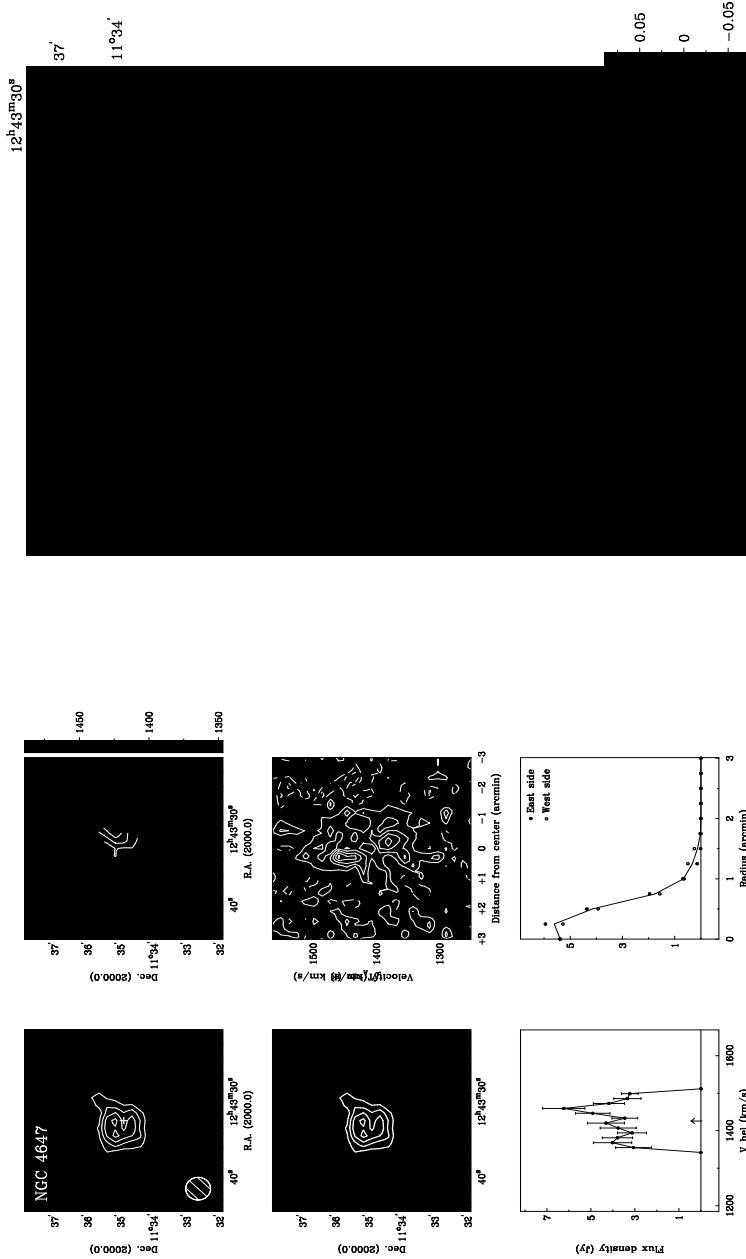


Fig. 12.— Group I-11. Same as Figure 2 for NGC 4647. In the optical image, the elliptical companion galaxy NGC 4649 is visible in the east.

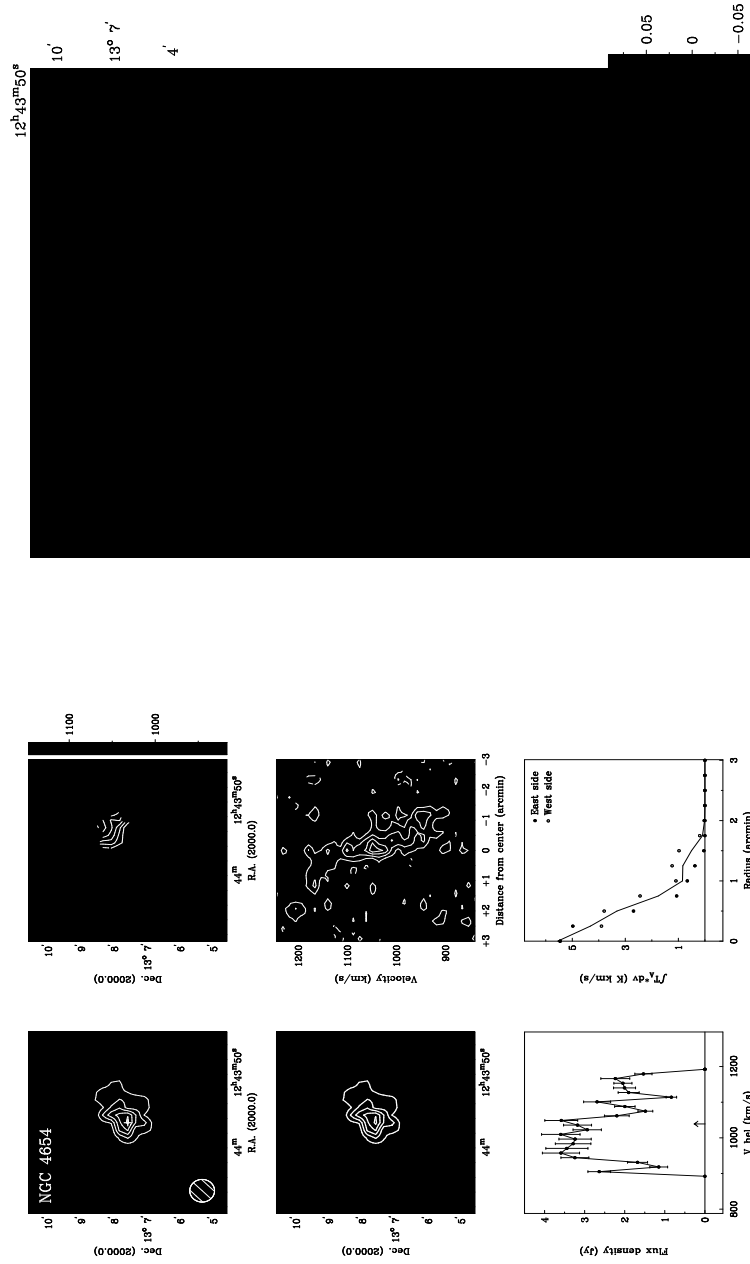


Fig. 13.— Group I-12. Same as Figure 2 for NGC 4654.

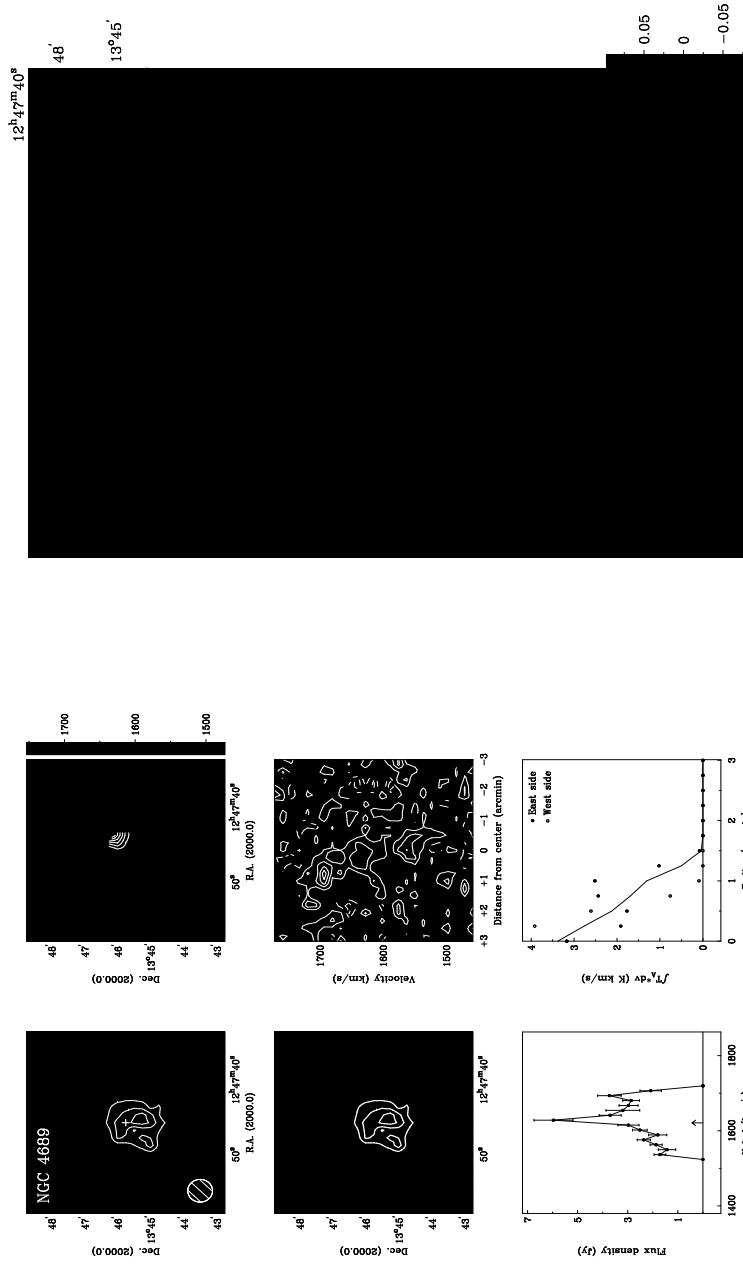


Fig. 14.— Group I-13. Same as Figure 2 for NGC 4689.

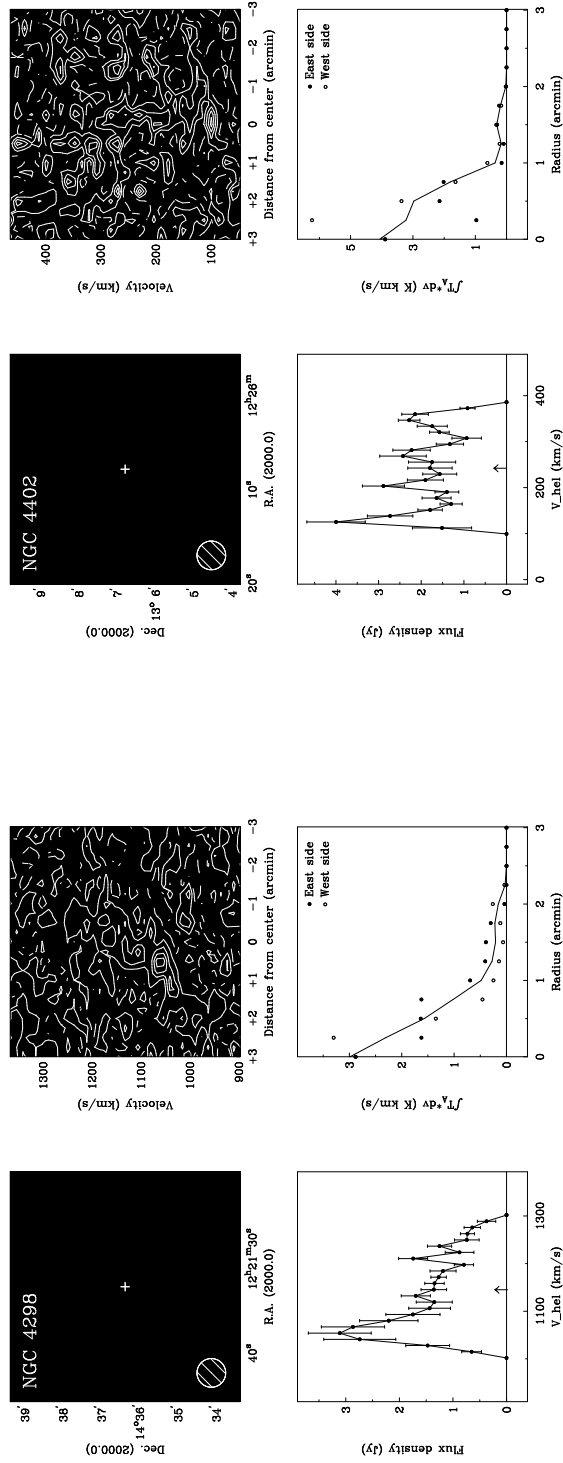


Fig. 15.— Group II-1. CO atlas of NGC 4298(left) and NGC 4402(right). Optical *B*-band image (top left), integrated position-velocity diagram (top right), global CO line profile (bottom left), and radial CO distribution (bottom right). In the optical image of NGC 4298, its companion galaxy NGC 4302 is visible in the west.

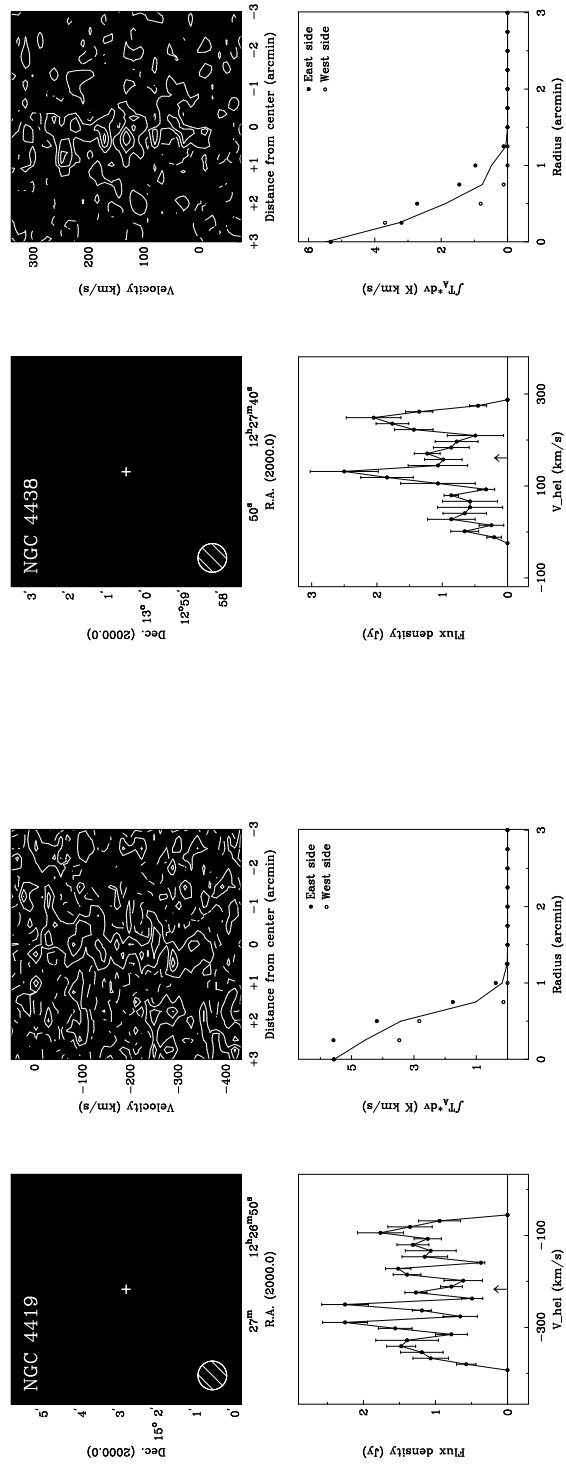


Fig. 16.— Group II-2. Same as Figure 15 for NGC 4419(left) and NGC 4438(right).

4.1. CO Atlas: Map Descriptions

Figures 2 – 17 are the CO atlas and selected channel maps of Group I and Group II galaxies obtained from our OTF mapping observations. The atlas figure for each Group I galaxy consists of 6 maps: a CO intensity map (top left), a velocity field map (top right), an optical image with CO contours (middle left), a position-velocity diagram derived along the major axis of the stellar disk (middle right), a global CO line profile (bottom left), and a radial CO profile (bottom right). Selected channel maps are also shown for Group I galaxies. For Group II galaxies, CO emission is too faint to yield an intensity map and velocity-field map. Therefore, only an optical *B*-band image from NASA/IPAC Extragalactic Database (NED³; top left), a position-velocity diagram derived by integrating along the minor axis (top right), a global CO line profile (bottom left), and a radial CO profile (bottom right) are shown.

Each map shown (including the channel maps) has a dimension of $6' \times 6'$ ($4' \times 4'$ for NGC 4536) since no emission was detected outside of this region for all galaxies. The velocity range shown for the global CO profile and channel map is about 500 km s^{-1} , except for NGC 4501 which has a CO line width of about 520 km s^{-1} . The contour levels shown are listed in Table 2.

CO intensity map: a CO intensity map is produced by summing all emission features in the channel maps. The contour levels shown are listed in K km s^{-1} , and the CO line intensity is in the T_{A}^* scale.

Velocity field map: a mean velocity field map is derived through single Gaussian fit to the observed line profiles.

Optical image: An optical *B*-band image is obtained from NED.

Position-velocity diagram: a PVD is extracted from a row of pixels along the major axis, i.e., a central slice of 15 arcsec width is shown in ATLAS, for Group I galaxies. For Group II galaxies, whose inclination is too high or whose CO emission is too weak in the individual channel maps, an integrated PVD is produced by summing the data along the minor axis. The integration is done over some minor axis length for each galaxy (1 or 2 beam-

³<http://nedwww.ipac.caltech.edu>

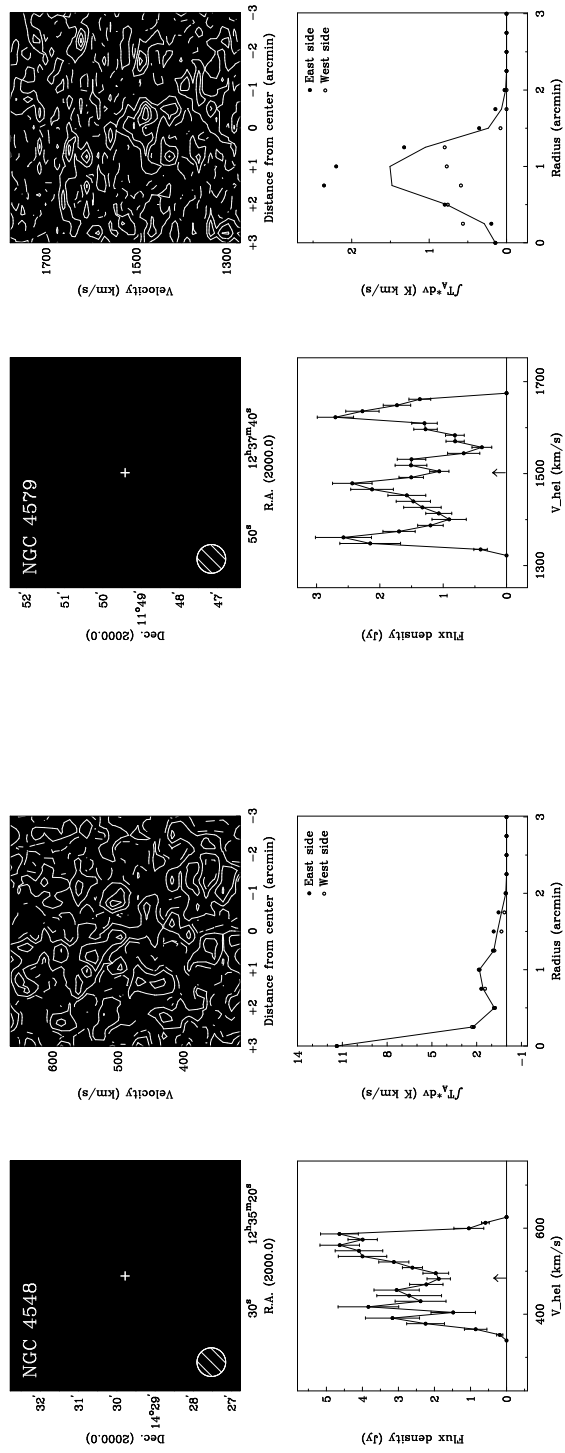


Fig. 17.— Group II-3. Same as Figure 15 for NGC 4548(left) and NGC 4579(right).

width for highly inclined galaxies and up to 7 beam-width for weak CO and face-on galaxies).

Global CO line profile: For Group I galaxies, a global CO line profile is extracted from the data cube. For the Group II galaxies, CO flux density is integrated manually along the minor axis of the PVD, and the global line profile is computed (e.g., Broeils & Rhee 1997; Rhee & Broeils 2005). The uncertainty in the integrated line flux in each channel is calculated as

$$\sigma_i^{\text{tot}} = \sqrt{\sigma_i^{\text{cal}2} + \sigma_i^{\text{rms}2} + \sigma_i^{\text{bsln}2}}, \quad (1)$$

$$\sigma_i^{\text{cal}} = T_i^* \times 0.1, \quad (2)$$

$$\sigma_i^{\text{rms}} = T_i^{\text{rms}}, \quad (3)$$

$$\sigma_i^{\text{bsln}} = \sqrt{(T_i^* - T_{i0})^2 + (T_i^* - T_{i1})^2 + (T_i^* - T_{i2})^2}, \quad (4)$$

where σ_i^{tot} is the total uncertainty, σ_i^{cal} , σ_i^{rms} , and σ_i^{bsln} are the calibration uncertainty, thermal noise in the channel maps, and the baseline subtraction noise. For the calibration uncertainty, we assign a 10% absolute uncertainty for all spectra following Kenney & Young (1988) (Eq. 2). T_i^* is CO line intensity, T_i^{rms} is map noise level, and T_{i0} , T_{i1} , and T_{i2} are CO intensities of the i -th channel derived by the baseline subtraction of 0, 1, and 2 order, respectively (see Kenney & Young 1988).

Radial CO profile: deriving a radial surface density profile using a concentric ellipse fitting method does not work well for edge-on or highly inclined galaxies. Warmels (1988) applied Lucy iteration method (Lucy 1974) to obtain HI radial surface density profile of edge on galaxies, and we derived radial CO profiles following Warmels (1988).

Channel map: The velocity range of each channel map is about 500 km s^{-1} (740 km s^{-1} for NGC 4501), which is the same as that of the global CO line profile.

4.2. CO Properties

CO properties for the 20 CO detected Virgo spiral galaxies are summarized in Table 3. The column entries are: (1) NGC number; (2) rms noise measured from emission-free regions; (3) line width measured at 20% level; (4) line width at 50% level; (5) systemic velocity derived from the CO velocity profile; (6) total CO line flux; (7) molecular hydrogen mass; (8) effective CO diameter; and (9) isophotal CO diameter.

Total CO flux & H₂ mass

To convert the CO intensity in T_{A}^* into the flux density unit, a calibration factor of 42 Jy K⁻¹ obtained using the FCRAO 14-m telescope (Kenney & Young 1988) is applied. We derive H₂ masses from total CO flux measured assuming a linear conversion relation (Kenney & Young 1989),

$$M_{\text{H}_2} = 3.9 \times 10^{-17} \chi d^2 S_{\text{CO}} (M_{\odot}) \quad (5)$$

where χ is the conversion factor and d is distance to the source in megaparsec (Mpc). We adopt $\chi = 3 \times 10^{20} \text{ cm}^{-2} (\text{K}[T_{\text{R}}] \text{ km s}^{-1})^{-1}$ (Young & Scoville 1991). The distance to the Virgo cluster is somewhat uncertain because of the large depth effect (Yasuda et al. 1997) and is generally thought to be between 15 and 20 Mpc (e.g., Young et al. 1995; Sakamoto et al. 1999; Sofue et al. 2003; Sandage & Tammann 2006; Mei et al. 2007). We adopt a distance of 20 Mpc for an easier comparison with the FCRAO Extragalactic CO Survey (see § 4.3).

CO line width

CO line width is measured at 20% and 50% level of the line peak, on each side of the line, following the definition of Rhee (1996). The line profile is divided into two equal velocity bins, and the peak fluxes $T_{\text{low}}^{\text{peak}}$ and $T_{\text{high}}^{\text{peak}}$ are determined separately on each half of the line profile. The 20% and 50% velocities ($V^{20\%}$ and $V^{50\%}$) represent the velocities at which the line profile reaches the 20% and 50% of the peak value on the respective high and low velocity side, approaching from the line edge to the center of the line profile. A linear interpolation procedure is used in this calculation.

The final value of line width of each cutoff-level is determined as

$$W_{20}^{\text{obs}} = V_{\text{high}}^{20\%} - V_{\text{low}}^{20\%} \quad (6)$$

$$W_{50}^{\text{obs}} = V_{\text{high}}^{50\%} - V_{\text{low}}^{50\%}. \quad (7)$$

The uncertainty in the line width is estimated with 1 σ uncertainty in each case where σ is a mean rms noise of line-free channels (Rhee & van Albada 1996).

The line width is corrected for instrumental broadening following the method described by Verheijen (1997). The correction for instrumental broadening (in km s⁻¹) is computed as

$$W_{20} = W_{20}^{\text{obs}} - 35.8 \left[\sqrt{1 + \left(\frac{\Delta V}{23.5} \right)^2} - 1 \right] \quad (8)$$

$$W_{50} = W_{50}^{\text{obs}} - 23.5 \left[\sqrt{1 + \left(\frac{\Delta V}{23.5} \right)^2} - 1 \right] \quad (9)$$

where ΔV is the velocity resolution in km s^{-1} .

CO systemic velocity

Again, following the procedure described by Verheijen (1997), we compute the systemic velocity of each galaxy as

$$V_{\text{sys}} = (V_{\text{low}}^{20\%} + V_{\text{high}}^{20\%} + V_{\text{low}}^{50\%} + V_{\text{high}}^{50\%}) / 4. \quad (10)$$

CO diameters

To describe CO extents, we derived effective diameters and isophotal diameters. Effective CO diameter, $D_{\text{CO}}^{\text{eff}}$, is defined as a diameter which encloses 70% of the total emission (see Young et al. 1995). The CO isophotal diameter, $D_{\text{CO}}^{\text{iso}}$, is defined as a diameter where the mean face-on surface density of H_2 falls to $1 \text{ M}_{\odot} \text{pc}^{-2}$ which corresponds to $\int T_R \text{ dv} = 0.21 \text{ K km s}^{-1}$, or $6.3 \times 10^{19} \text{ H}_2 \text{ cm}^{-2}$ for a CO– H_2 proportionality factor of $\chi = 3 \times 10^{20} \text{ cm}^{-2} (\text{K}[\text{T}_R] \text{ km s}^{-1})^{-1}$ (Young & Scoville 1991).

4.3. Comparison With Other Observations

Previous single dish and interferometric CO measurements exist for many of our target galaxies. A comparison of our results with those of the FCRAO Extragalactic CO Survey (Young et al. 1995) and the BIMA SONG (Helfer et al. 2003) provides an important test of potentially important systematics associated with these two widely utilized extragalactic CO surveys.

4.3.1. Comparison With the FCRAO Extragalactic CO Survey

The FCRAO extragalactic CO survey (Young et al. 1995) data on 300 external galaxies is the most extensive and most widely referenced database for CO emission measurements in 300 external galaxies. A comparison with our CO imaging survey of Virgo cluster spirals provides an important verification of this earlier survey, which employed sampling and modeling rather than full imaging, and offers a quantitative constraint on the systematics resulting from the emission modeling used by Young et al. in estimating the total CO luminosity. Since both surveys used the same telescope and calibration method as well as adopting the identical distance to the Virgo Cluster, any hardware-dependent systematics are minimized. Therefore any measured difference is narrowly constrained to the differences in the observing methods and the modeling used by Young et al. NGC 4536 is excluded in this comparison because the small area coverage of our maps may have adversely affected the baseline subtraction process.

Table 3. Derived CO Properties

Galaxy	rms (K)	W_{20}^a (km s ⁻¹)	W_{50}^b (km s ⁻¹)	V_{sys}^c (km s ⁻¹)	S_{CO} (Jy km s ⁻¹)	M_{H_2} (10 ⁸ M _⊙)	$D_{\text{CO}}^{\text{eff } d}$ (arcmin)	$D_{\text{CO}}^{\text{iso } e}$ (arcmin)
Group I								
NGC 4254	0.016	221±1	209±4	2392	2830±290	134±14	2.6	5.1
NGC 4302	0.013	353±1	344±4	1147	540±150	25±7	2.7	3.6
NGC 4303	0.018	162±2	145±4	1566	1920±200	90±9	2.2	3.9
NGC 4321	0.021	239±2	217±4	1580	2390±270	113±13	1.8	4.5
NGC 4501	0.017	518±2	502±3	2276	2130±240	101±11	2.5	4.8
NGC 4527	0.017	376±2	358±5	1736	1260±160	60±7	1.7	3.4
NGC 4535	0.029	252±5	235±5	1960	1450±250	68±12	2.3	3.9
NGC 4536*	0.010	318±2	267±5	1802	390±50	19±3	0.8	1.9
NGC 4567**	0.018	297±3	272±4	2242	1500±170	71±8		
NGC 4569	0.022	311±1	297±5	-219	900±130	43±6	1.3	2.9
NGC 4647	0.016	156±1	145±12	1426	620±100	29±5	1.2	2.8
NGC 4654	0.014	285±1	270±5	1039	710±90	33±4	1.8	3.4
NGC 4689	0.020	182±1	171±3	1621	510±80	24±4	1.6	2.8
Group II								
NGC 4298	0.012	270±4	214±10	1145	410±60	20±3	2.1	3.6
NGC 4402	0.025	267±3	251±5	242	520±100	24±5	1.4	1.5
NGC 4419	0.016	318±2	290±13	-218	390±100	18±5	0.9	2.0
NGC 4438	0.018	272±5	151±8	161	300±70	14±3	1.1	2.3
NGC 4548	0.015	234±6	217±5	484	710±90	34±4	2.1	3.7
NGC 4579	0.014	329±1	317±5	1502	500±70	23±3	2.1	3.1

Note. — ^{a,b} Linewidths are corrected for the instrumental broadening (see Eqs. 8 & 9). Uncertainties are derived by following Rhee & van Albada (1996).

^c CO systemic velocity

^d Diameter which contains 70% of the total CO flux

^e Diameter where the mean face-on surface density of H₂ falls to 1 M_⊙ pc⁻². H₂ surface density distribution (in unit of M_⊙ pc⁻²) is derived from CO radial distribution (in unit of K km s⁻¹) assuming a constant CO to H₂ conversion factor within a whole galaxy ($\chi = 3 \times 10^{20} \text{ cm}^{-2} (\text{K}[\text{T}_R] \text{ km s}^{-1})^{-1}$ (Young & Scoville 1991)).

* CO properties of NGC 4536 is derived from the datacube mapped by 6' × 4' size.

**The entries for NGC 4567 are the total values for NGC 4567 and NGC 4568 as a pair. CO diameters are not given for these galaxies.

Table 4. Comparison with Young et al. (1995)

Galaxy	FCRAO 14-m (OTF) ^a			FCRAO 14-m (Position Switching) ^b					
	$S_{\text{CO}}^{\text{OTF}}$ (Jy km s ⁻¹)	$D_{\text{iso}}^{\text{OTF}}$ (arcmin)	$D_{\text{eff}}^{\text{OTF}}$ (arcmin)	$S_{\text{CO}}^{\text{PS.fit}}$ (Jy km s ⁻¹)	scf (%)	$S_{\text{CO}}^{\text{PS.obs}}$ (Jy km s ⁻¹)	$D_{\text{iso}}^{\text{PS.fit}}$ (arcmin)	$D_{\text{eff}}^{\text{PS.fit}}$ (arcmin)	r (%)
(1)	(2)	(3)	(4)	(5)	(6)	(7)	(8)	(9)	(10)
Group I									
NGC 4254	2830±290	5.4	2.6	3000±850	37	1110	5.3	3.4	6
NGC 4302	540±150	4.6	2.7	620±100	100	620	2.0	1.8	15
NGC 4303	1920±200	4.2	2.2	2280±470	50	1140	3.4	2.2	19
NGC 4321	2390±270	5.4	1.8	3340±920	39	1300	4.5	3.4	40
NGC 4501	2130±240	5.2	2.5	2220±480	59	1310	3.8	2.9	4
NGC 4527	1260±160	3.8	1.7	1800±410	92	1660	3.4	2.0	43
NGC 4535	1450±250	4.1	2.3	1570±410	38	600	3.9	3.5	8
NGC 4567 *	1500±170			1550±210	81	1250			3
NGC 4569	900±130	3.1	1.3	1500±260	82	1230	3.2	1.8	67
NGC 4647	620±100	3.2	1.2	600±120	66	400	2.2	1.6	-3
NGC 4654	710±90	3.6	1.8	730±150	62	450	2.6	2.4	3
NGC 4689	510±80	3.0	1.6	710±150	50	360	2.4	2.4	39
Group II									
NGC 4298	410±60	1.5	2.1	660±110	86	570	2.4	1.8	61
NGC 4402	520±100	1.8	1.4	630±120	98	620	2.4	1.4	21
NGC 4419	390±100	1.5	0.9	920±190	91	840	2.2	1.4	136
NGC 4438	300±70	1.4	1.1	210±40	94	200	1.3	1.2	-27
NGC 4548	710±90	2.4	2.1	540±140	60	320	3.3	3.0	-24
NGC 4579	500±70	2.5	2.1	910±200	47	430	2.7	2.6	82

Note. — ^a Our new OTF observation results

^b Position-Switching observation results by Young et al. (1995)

Col. (1) — NGC number

Col. (2) — Total CO flux, $S_{\text{CO}}^{\text{OTF}}$, and its rms, σ_{OTF} , derived from our OTF observations

Col. (3) & (4) — The isophotal and effective CO diameter, $D_{\text{iso}}^{\text{OTF}}$ and $D_{\text{eff}}^{\text{OTF}}$, derived from our OTF observation. To compare with Young et al. (1995), $D_{\text{iso}}^{\text{OTF}}$ in here is derived at the diameter where the face-on CO integrated intensity falls to 1 K(T_{Λ}^*) km s⁻¹.

Col. (5) — The fitted total CO flux, $S_{\text{CO}}^{\text{PS.fit}}$, and its rms, σ_{fit} , by Young et al. (1995)

Col. (6) — Scale factor which is the percentage of the total CO emission sampled by the observations by Young et al. (1995)

Col. (7) — Recomputed Young et al. PS observed CO flux, $S_{\text{CO}}^{\text{PS,obs}}$, using Col. (5) and Col. (6).

Col. (8) & (9) — The isophotal and effective CO diameter, $D_{\text{iso}}^{\text{PS,fit}}$ and $D_{\text{eff}}^{\text{PS,fit}}$, which is the diameter where the face-on CO integrated intensity falls to $1 \text{ K}(T_{\text{A}}^*) \text{ km s}^{-1}$ and the diameter which contains 70% of the total CO flux for the best-fitting model, respectively (Young et al. 1995).

Col. (10) — Fractional ratio of the difference between $S_{\text{CO}}^{\text{OTF}}$ and $S_{\text{CO}}^{\text{PS,fit}}$, calculated as $(S_{\text{CO}}^{\text{PS,fit}} - S_{\text{CO}}^{\text{OTF}})/S_{\text{CO}}^{\text{OTF}} \times 100$.

* NGC 4567 and NGC 4568 cannot be separated in our OTF observations, and the summed total flux is reported. For the PS results, the equivalent summed CO flux of NGC 4567 and NGC 4568 is listed (Young et al. 1995).

A comparison of the FCRAO 14-m OTF and PS measurements are summarized in Table 4. Both the raw PS ($S_{\text{CO}}^{\text{PS,obs}}$) and the model fit ($S_{\text{CO}}^{\text{PS,fit}}$) results are listed, using the scale factor (scf) given in the original paper (Young et al. 1995). An isophotal diameter $D_{\text{iso}}^{\text{OTF}}$ is defined as the diameter where the face-on CO integrated intensity falls to $1 \text{ K}(T_{\text{A}}^*) \text{ km s}^{-1}$ while an effective diameter $D_{\text{eff}}^{\text{OTF}}$ is defined as the diameter which contains 70% of the total CO flux, following the definition by Young et al.(1995). The fractional ratio between the OTF and PS measurements, r , is calculated and presented to show the difference between the two methods of the total CO flux. Comparisons of the OTF and PS measurements are also shown in Figure 18.

The panel (A) in Figure 18 shows that the observed PS line fluxes are systematically smaller than the OTF measurements, but this is expected since “observed PS” data include only partial measurements taken along the major axis. A better agreement is expected for galaxies with a high inclination and a small size. And indeed galaxies with a smaller D_{25} and a larger inclination appears to have a smaller discrepancy between $S_{\text{CO}}^{\text{PS,obs}}$ and $S_{\text{CO}}^{\text{OTF}}$. The model-fit measurements shown in panel (B) are more consistent with the OTF measurements. The OTF and PS model-fit measurements of 9 galaxies are consistent with the total CO flux to within 1σ . Out of the remaining 9 galaxies, 7 show larger $S_{\text{CO}}^{\text{PS,fit}}$ than $S_{\text{CO}}^{\text{OTF}}$ by a factor of 1.4 - 2.4. And, the last two galaxies (NGC 4438 and NGC 4548) have larger $S_{\text{CO}}^{\text{OTF}}$ than $S_{\text{CO}}^{\text{PS,fit}}$ by a factor of 1.4. Among the 9 galaxies for which the discrepancies are larger than 1σ , there are 4 galaxies which disagree by $\geq 2\sigma$ uncertainty, and the 4 galaxies have larger $S_{\text{CO}}^{\text{PS,fit}}$ than $S_{\text{CO}}^{\text{OTF}}$ by a factor of 1.6 - 2.4. We predict that peculiar CO distributions such as ring- or bar-like structures (e.g., Young et al. 1995) can affect the model fitting process, and more analysis will be done in another paper (Chung et al. 2010).

Panels (C) and (D) in Figure 18 show the comparisons of CO diameters derived from the OTF and PS observations. For Group I galaxies detected with high S/N ratio, isophotal diameters derived from the OTF data ($D_{\text{iso}}^{\text{OTF}}$) are larger than those of the PS data ($D_{\text{iso}}^{\text{PS,fit}}$). In contrast, the effective diameters of OTF ($D_{\text{eff}}^{\text{OTF}}$) are smaller than $D_{\text{eff}}^{\text{PS,fit}}$. An explanation for these apparently puzzling trends is that CO emission is spread over a larger extent but has a more concentrated central component in the OTF maps when compared with the results of Young et al. (1995). The effective diameters $D_{\text{eff}}^{\text{OTF}}$ are smaller than 3 arcmin in every case, and the isophotal diameters are located between 1/2 and 1 of the optical diameter D_{25} in most cases. $D_{\text{iso}}^{\text{OTF}}$ for Group II galaxies are systematically smaller than $D_{\text{iso}}^{\text{PS,fit}}$, and this may be the result of low S/N ratios of the OTF data.

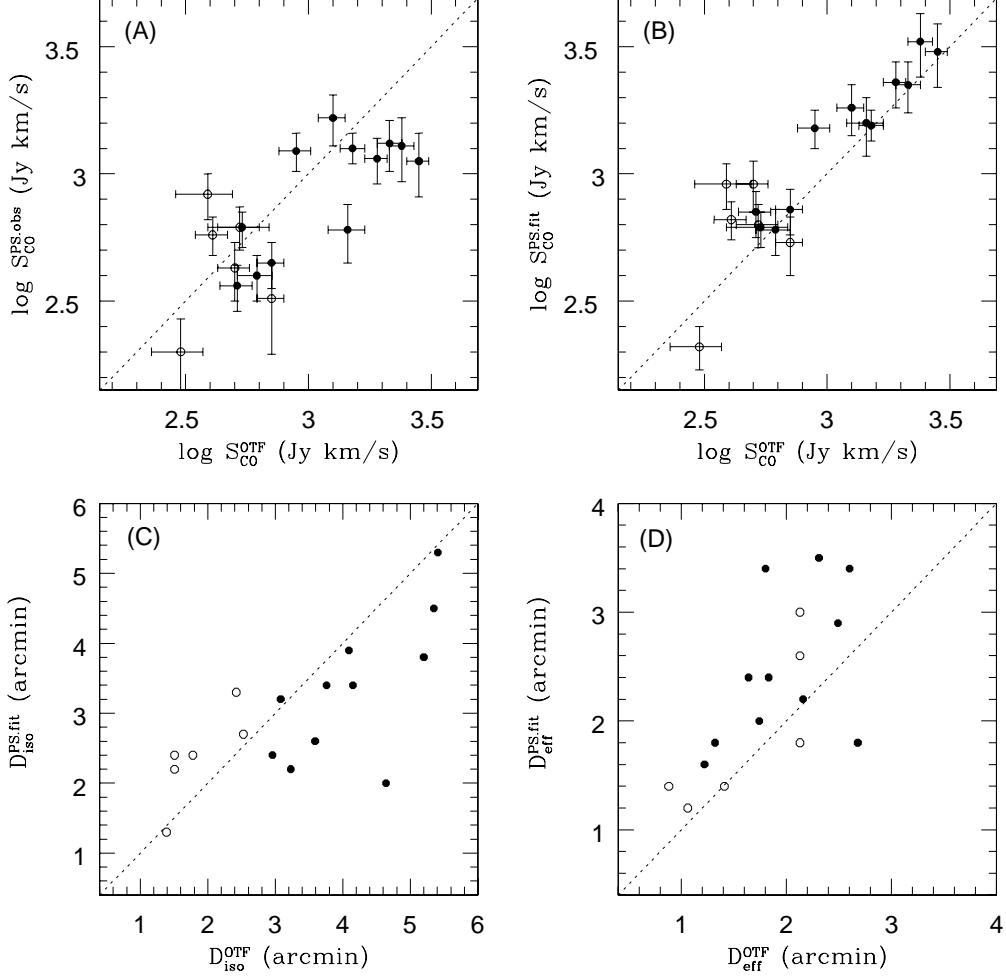


Fig. 18.— Comparison of the data with the FCRAO extragalactic CO survey (Young et al. 1995). Here, “PS” denotes the position-switch measurements reported in the FCRAO extragalactic CO survey data while “OTF” refers to our On-the-Fly data. Panel (A) compares the total CO fluxes of the OTF measurements with the PS measurements. Panel (B) compares the total CO fluxes of the OTF measurements with the model fit corrected PS data. Panels (C) and (D) compare the isophotal and effective diameters derived from the OTF and the PS data, respectively. Isophotal diameters $D_{\text{iso}}^{\text{OTF}}$ and $D_{\text{iso}}^{\text{PS.fit}}$ are defined as the diameter where the face-on CO integrated intensity falls to $1 \text{ K}(T_{\text{A}}^*) \text{ km s}^{-1}$. Effective diameters $D_{\text{eff}}^{\text{OTF}}$ and $D_{\text{eff}}^{\text{PS.fit}}$ are the diameter which contains 70% of the total CO flux. The dotted line represents a perfect linear relationship. Filled and open symbols denote Group I and Group II galaxies, respectively.

4.3.2. Comparison With the BIMA SONG Survey

Three galaxies imaged in the OTF mode (NGC 4303, NGC 4321, & NGC 4569) were also observed by the BIMA SONG project (Helfer et al. 2003). The total BIMA SONG CO fluxes reported for NGC 4303, NGC 4321, and NGC 4569 are 2427 ± 145 , 2972 ± 319 , and 1096 ± 137 Jy km s⁻¹, respectively. These integrated CO line fluxes are systematically slightly larger ($\sim 25\%$) compared with our OTF measurements and are between the OTF and PS measurements on average. The apparent difference may be rooted in the systematic difference in calibration. Because of the small number of objects in common, we can only report a broad agreement.

5. DISCUSSION

5.1. Notes on Individual Galaxies

In this section, we offer supplementary information on the individual galaxies and offer comparisons with other CO, HI, and H α observations. In particular, we are interested in the environmental influence on the molecular ISM, and we make notes of any peculiar CO distribution that may be related to the cluster environment.

5.1.1. Group I Galaxies

NGC 4254: This Sc galaxy is located 3.3° northwest of M87. Cayatte et al. (1990) reported that it has a very asymmetric HI distribution with a sharp edge on the side pointing toward M87 and an extended HI feature pointing away from M87, as if it were compressed by the intergalactic medium. In our CO intensity map, CO appears to extend to the south. Chemin et al. (2006) showed an asymmetric structure in H α velocity field. Streaming motions along the spiral arms and steep velocity rise are observed in their atlas. Our CO velocity field map and position-velocity diagram are in good agreement with the H α kinematics. Interferometric high resolution imaging of the central region shows clumped CO distribution along the spiral arms, a bar-like elongation feature, and slight depression at the dynamical center (Sakamoto et al. 1999; Sofue et al. 2003).

NGC 4302: This Sc galaxy is a dusty edge-on spiral located 3.1° northwest of M87. Its

CO distribution in our CO intensity map consists of two molecular peaks with a central depression. Young et al. (1995) modeled the CO distribution as being offset by $0'.45$ from its center. Our new data suggest that this earlier study might have detected only one of the two peaks.

NGC 4303: This Sc spiral is located 8.2° south of M87. Cayatte et al. (1990) reported a symmetric HI distribution with a central depression. Our atlas shows that CO emission is distributed along the spiral arms, and a bar-like structure is displaced in position angle by about 20 degrees. Helfer et al. (2003) reached the same conclusion using the BIMA SONG survey data. The CO emission is concentrated in the central region, unlike the HI (see Cayatte et al. 1990), but the HI and CO velocity fields are in good agreement. A recent burst of star formation caused by tidal interactions with two nearby companions has been suggested by Cayatte et al. (1990).

NGC 4321: This Sc galaxy is located 3.9° north of M87. Its HI emission is distributed along the spiral arms, and the oval distortion in the inner part due to the presence of a bar is shown from the kinematic pattern (Cayatte et al. 1990). Our CO image shows a well confined CO distribution on the stellar disk, plus an asymmetric extension to the southern spiral arm. It also has an elongated bar like structure along the major axis. The CO velocity field shows an oval distortion in the inner part, similar to the HI (Cayatte et al. 1990). The BIMA SONG survey detected CO at the center and along the spiral arms (Helfer et al. 2003), in a good agreement with our results. Sakamoto et al. (1999) reported a prominent pair of nuclear CO arms and a sharp condensation of CO at the nucleus. Chemin et al. (2006) found three different pattern speeds, which is a sign of a streaming motion.

NGC 4501: This Sbc spiral is located 2.1° north of M87. Cayatte et al. (1990) reported that this galaxy points its steep HI edge toward M87, similar to NGC 4254, and suggested these two galaxies as examples of enhanced star formation caused by compression of the ISM. Our CO intensity map shows a well-centered distribution. Sakamoto et al. (1999) reported a concentrated CO morphology, and Sofue et al. (2003) found that the north-eastern arm is much brighter in CO than the south-western arm. The CO velocity width of NGC 4501 is one of the largest among the galaxies observed. The $H\alpha$ velocity field appears regular, but the position-velocity diagram shows a complex kinematics (Chemin et al. 2006).

NGC 4527: This Sb galaxy is located 9.8° south of M87. Kenney & Young (1988) reported that it has a uniform disk component. Our OTF map is consistent with the Young et al.

data, but the OTF map shows that there is a central CO concentration along with a bar along the major axis and an asymmetric extension to the southwest.

NGC 4535: This SBc spiral is located 4.3° south of M87. This galaxy shows an undisturbed HI distribution with a central hole (Cayatte et al. 1990). Helfer et al. (2003) reported that CO is distributed at the center and along the spiral arms. Sofue et al. (2003) classified this galaxy as a typical single-peak type with offset bars. Our OTF data is noisy, and the signal is very weak. The CO intensity map shows a bar-like elongated structure in the central region, and the position-velocity diagram shows evidence for highly disturbed gas kinematics. Chemin et al. (2006) reported a perturbed velocity field and streaming motions along the arms.

NGC 4536: This Sc galaxy is located 10.2° south of M87. Our map covers only a $6' \times 4'$ region, but the CO emission appears to be fully covered when compared with the CO map of Kenney & Young (1988). CO emission is strongly concentrated on the galactic center, and this agrees well with the results by Sofue et al. (2003).

NGC 4567 & 4568: These two Sc galaxies are located 1.8° , and they are not well separated spatially or kinematically. Cayatte et al. (1990) suggested that the HI emission displaced toward the south of NGC 4567 could be a sign of a tidal interaction between the two galaxies. Koopmann & Kenney (2004) also suggested ram pressure effects and a tidal interaction between the two. However, $H\alpha$ velocity field does not show any clear signs of velocity disturbances (Chemin et al. 2006). Higher angular resolution HI and CO observations by Iono et al. (2005) also show that the inner gas disks show little signs of tidal disturbance, with a symmetric bar-like or spiral-like features. Unlike many other observed Virgo galaxies, they both show CO emission extending out to the outer optical radii in our OTF map, including where the two disks overlap.

NGC 4569: This Sab spiral is an HI-anemic galaxy (van den Bergh 1976) located 1.7° northeast of M87. Cayatte et al. (1990) reported that its HI disk is severely stripped. Interferometric CO imaging found a symmetric CO distribution with two peaks and a central depression (Helfer et al. 2003; Sofue et al. 2003). Higher resolution CO imaging by Nakanishi et al. (2005) found a highly concentrated CO distribution in the circum-nuclear region with two off-center peaks. Our CO atlas shows a centrally concentrated distribution with a much smaller CO radius than the optical radius and a bar-like elongated structure across the optical major axis. Its $H\alpha$ velocity field is perturbed and shows evidence for

streaming motions (Chemin et al. 2006). Our CO velocity field map shows that central velocity is shifted toward the south.

NGC 4647: This Sc galaxy is located 3.2° east of M87 and has a companion elliptical galaxy NGC 4649. NGC 4647 shows a slightly extended HI distribution toward NGC 4649 (Cayatte et al. 1990). However, CO appears to point away from its elliptical companion NGC 4649 in our intensity map. The CO position-velocity diagram also appears disturbed. The companion galaxy NGC 4649 is undetected in CO.

NGC 4654: This SBc galaxy is located 3.3° northeast of M87. The HI image shows a sharp cutoff on the northwest side and an eastward extension, and enhanced star formation activity is also seen in the northwest (Cayatte et al. 1990). Kenney & Young (1988) found an asymmetric CO distribution – the position $45''$ northwest of the nucleus shows a stronger line than the central $45''$, and this region also displays a peak in the HI, radio continuum, and the $H\alpha$. Sofue et al. (2003) found a lopsided CO distribution in the inner region and suggested that even the nuclear region suffers from the ram pressure effects. Our OTF CO maps also shows a clear asymmetry and lopsidedness, but the CO peak is well centered on the stellar disk. The lopsided CO extension is both to the northwest and to the southwest, in the direction of M87. The $H\alpha$ velocity field is strongly perturbed (Chemin et al. 2006).

NGC 4689: This Sc galaxy is located 4.3° northeast of M87. It has a large, extended HI disk (Cayatte et al. 1990). High angular resolution CO imaging by Sofue et al. (2003) found a lopsided, amorphous CO morphology and without a central peak. Our CO map shows a CO peak offset from the optical center and extended to the south. Chemin et al. (2006) reported that $H\alpha$ velocity field is slightly perturbed due to streaming associated with pseudo-spiral arms.

5.1.2. *Group II Galaxies*

NGC 4298: This Sc galaxy is located 3.2° northwest of M87 and has a companion NGC 4302 only 2.3 arcmin away. Stellar asymmetry due to a recent tidal interaction is seen in optical images, and a truncated gas disk due to ram-pressure is also suggested (Koopmann & Kenney 2004). Chemin et al. (2006) suggested that its mildly perturbed velocity field may indicate a streaming motion or a locally warped arm. Our PVD shows stronger emission on the east

(receding) side than on the west (approaching) side, and CO emission is probably extended toward southeast side, in the direction of its companion galaxy NGC 4302. This feature is in good agreement with the H α kinematics discussed above.

NGC 4402: This edge-on Sc galaxy is located 1.4° northwest of M87. Although the high velocity part of the HI emission is missed by Cayatte et al. (1990), it is obvious that the HI disk of this galaxy is significantly smaller in extent than that of the optical disk. Our CO position-velocity diagram shows that CO emission is asymmetric to one side, and Young et al. (1995) also suggested the distribution model to be offset by $0'.20$ from the center. A $10''$ radius nuclear disk and a more extended molecular disk with a $30''$ diameter are found by higher angular resolution observations (Sofue et al. 2003).

NGC 4419: This Sa galaxy is located 2.8° north of M87. Kenney & Young (1988) proposed that NGC 4419 is on a radial orbit which passes very close to the cluster core and strongly interacts with the intracluster medium, resulting in a large CO/HI flux ratio and a significant CO asymmetry. CO distribution model of Young et al. (1995) shows an offset $0'.25$ from center, and Sofue et al. (2003) reported that the outer molecular disk is lopsided toward the northwest. Our CO position-velocity diagram shows a compact distribution and a rapidly rising rotation speed in the central region.

NGC 4438: This Sb galaxy is located 1.0° northwest of M87. Cayatte et al. (1990) reported a highly asymmetric HI distribution with an extension pointing , and a much smaller HI disk than the optical disk. Its ionized gas has an off-plane filamentary morphology to the east and south of the disk (Chemin et al. 2006; Kenney et al. 1995; Kenney & Yale 2002). Our CO position-velocity diagram shows that its molecular center is offset from the optical center by ~ 0.5 arcmin to the east. It also shows a highly disturbed structure.

NGC 4548: This SBb galaxy is located 2.4° northeast of M87. This galaxy is a nearly face-on barred (SBb) spiral which is severely HI-deficient (van den Bergh 1976; Giovanelli & Haynes 1983). Cayatte et al. (1990) reported a ring structure in the HI distribution. The BIMA SONG survey detected CO only at the center (Helfer et al. 2003), and Sofue et al. (2003) also reported a very weak and highly concentrated CO distribution. Our CO data is weak and too noisy to determine the molecular distribution well. However, its global CO line profile shows moderately symmetric double horns and CO appears to have comparatively large extent from the integrated PVD and radial profile.

NGC 4579: This Sab galaxy is located 1.8° east of M87 and is another HI-anemic spiral (van den Bergh 1976). Its HI distribution shows a ring-like structure, and it is the most severely stripped galaxy with signs of unusual nuclear activity, possibly fueled by gas inflow (Cayatte et al. 1990). The BIMA SONG survey detected CO only at the center (Helfer et al. 2003), and Sofue et al. (2003) reported that elongated CO distribution is displaced from the optical bar axis by about 30 degrees. Its $H\alpha$ velocity field shows evidence for perturbed, streaming motions (Chemin et al. 2006). Our CO position-velocity diagram shows a severely disturbed morphology and kinematics.

5.2. Summary of CO distribution

Here, we summarize the CO distribution of the Virgo spiral galaxies shown by our survey.

1. CO is confined to the galactic center and disk in most galaxies. However, slight asymmetric distribution and significant structures as well as kinematic disturbances are frequently shown. This is consistent with previous results of CO studies (e.g., Young et al. 1995; Helfer et al. 2003).
2. Among the 14 galaxies which have CO intensity maps, 11 galaxies have single CO peak center (NGC 4254, NGC 4303, NGC 4321, NGC 4501, NGC 4527, NGC 4535, NGC 4536, NGC 4567, NGC 4568, NGC 4569, and NGC 4654). NGC 4302 has twin peaks with a central depression, and NGC 4647 and NGC 4689 have no notable CO peak at the center.
3. Five galaxies appear to have bar-like elongated structure (NGC 4303, NGC 4321, NGC 4527, NGC 4535, and NGC 4569). Extended CO distributions to one side are also seen in 6 galaxies (NGC 4254, NGC 4298, NGC 4527, NGC 4654, NGC 4689, and NGC 4402).
4. CO emission in NGC 4298 shows an asymmetric extension toward the southeast, which is the direction of its companion galaxy NGC 4302. NGC 4647 shows a CO distribution pointing away from its elliptical companion NGC 4649.

Figure 19 shows the total CO extent and morphology of each of the 14 Group I galaxies at their proper position in the Virgo cluster. There are several noteworthy trends:

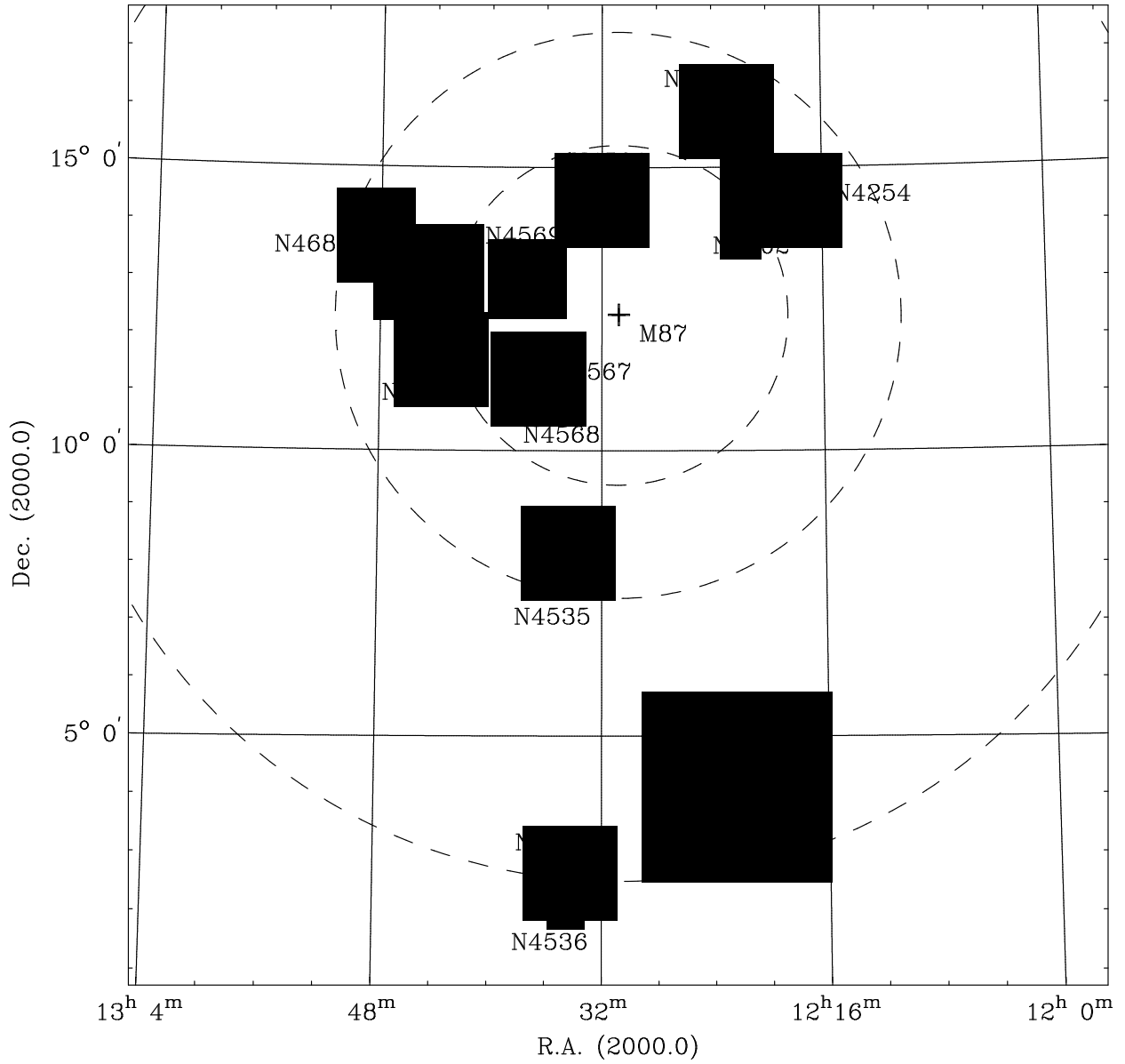


Fig. 19.— Spatial distribution of the 14 Group I galaxies in the Virgo Cluster. Individual galaxies are 20 times enlarged to be shown more clearly. Contour levels correspond to a H₂ column density of 0.75, 1.50, 2.25, and 3.00 10²⁰ cm⁻². The radius of each dashed circle is 3, 5, and 10 degrees, respectively.

1. It appears that CO molecules are not strongly affected by the cluster environments such as distance from the cluster center of M87.
2. Galaxies located in the western side of Virgo Cluster are known to have a larger HI disk than the galaxies in the eastern side (Cayatte et al. 1990), and we find the same trend in the CO disk size as well.
3. NGC 4298 and NGC 4647 have companion galaxies, but CO emission is extended toward and on the opposite to its companion, respectively. Figure 19 suggests that both of their extensions point toward the cluster center near M87. NGC 4654 also shows a CO extension toward M87.

6. SUMMARY & CONCLUDING REMARKS

We have carried out a $^{12}\text{CO}(J=1-0)$ OTF mapping survey of 28 Virgo cluster spiral galaxies. Although the importance of molecular contents in galaxy evolution is widely recognized, systematic CO imaging surveys of a large galaxy sample covering the full extent of the stellar disks are still rare. Taking advantages of the OTF mapping mode of the FCRAO 14-m telescope, we have imaged a large area of each galaxy covering the entire stellar disks in a relatively short period of time compared with the more traditional position-switched grid-map mode.

We detected and mapped CO emission in 20 of the galaxies with uniform sensitivity. Here we present their global CO properties. The CO emission is generally well centered on the stellar disk. However, some Virgo spirals show extended CO distribution to one side or bar-like CO distribution. The comparison of our CO data with those of the FCRAO extragalactic CO survey (Young et al. 1995) suggests that the major axis scan and global modeling used by Young et al. was largely successful in estimating the total CO luminosity. Young et al. has larger CO luminosities than our results for 7 (4) out of 18 galaxies by 1σ (2σ) uncertainty. Further analysis of these data will be presented in our future papers. Extensive multi-wavelength data are now available for joint-analysis with our new CO data, including the HI (Chung et al. 2007), radio (Yun, Reddy, & Condon 2001), IR (Spitzer & Akari), optical (HST & SDSS), $\text{H}\alpha$ (Koopmann & Kenney 2004), and UV (GALEX). We will examine radial dependence of the star formation rate and star formation efficiency. Their dependence on the morphological type, luminosity, and environments will also be studied using the global CO properties. To study environmental effects in different cluster evolutionary stages, we will use our Virgo data with the OTF mapping data of Ursa Major cluster spiral galaxies (Chung et al. 2010) and single dish spectra of the Pisces filament spiral galaxies (Lee et al. 2010) obtained using the Kitt Peak 12-m telescope. We will also explore the utility of the

CO Tully-Fisher relation.

We thank A. Chung for valuable comments and discussions. We would also like to thank T. Jung and H. Kang for excellent support at the data reduction process and the system. Thoughtful comments from the anonymous referee are appreciated. This work was supported in part by NSF grants AST 0096854 and AST 0540852.

REFERENCES

- Boselli, A., & Gavazzi, G. 2006, *PASP*, 118, 517
- Broeils, A. H., & Rhee, M.-H. 1997, *ApJS*, 111, 143
- Brosch, N. et al., 1997, *ApJS*, 111, 143
- Cayatte, V. et al., 1990, *AJ*, 100, 604
- Chemin, L. et al., 2006, *MNRAS*, 366, 812
- Chung, A. 2007, PhD Thesis, Columbia University
- Chung, A., van Gorkom, J. H., Kenney, J. D. P., & Vollmer, B. 2007, *ApJ*, 659, L115
- Chung, A. et al., 2010, *ApJ*, in preparation
- Chung, E. J., Kim, H., & Rhee, M.-H. 2005a, *JKAS*, 38, 17
- Chung, E. J., Kim, H., & Rhee, M.-H. 2005b, *JKAS*, 38, 371
- Chung, E. J., Kim, H., & Rhee, M.-H. 2006, *JASS*, 23, 269
- Chung, E. J. et al., 2010, *JASS*, in preparation
- Condon, J. J. et al., 1998, *AJ*, 115, 1693
- Cote, P. et al., 2004, *ApJS*, 153, 223
- Dale, D. A. et al., 2007, *ApJ*, 655, 863
- Giovanelli, R., & Haynes, M. P. 1983, *AJ*, 88, 881
- Giovanelli, R. et al., 2007, *AJ*, 133, 2569

- Helfer, T. T. et al., 2003, *ApJS*, 145, 259
- Iono, D., Yun, M. S., & Ho, P. T. P. 2005, *ApJS*, 158, 1
- Kenney, J. D. P., & Young, J. S. 1988, *ApJS*, 66, 261
- Kenney, J. D. P., & Young, J. S. 1989, *ApJ*, 344, 171
- Kenney, J. D. P. et al., 1995, *ApJ*, 438, 135
- Kenney, J. D. P., & Yale, E. E. 2002, *ApJ*, 567, 865
- Kenney, J. D. P. et al., 2008, *The Evolving ISM in the Milky Way & Nearby Galaxies*, ed. K. Sheth, A. Noriega-Crespo, J. Ingalls, & R. Paladini, published online at heep://ssc.spitzer.caltech.edu/mtgs/ismevol/ (arXiv:0803.2532)
- Koopmann, R. A., & Kenney, J. D. P. 2004, *ApJ*, 613, 866
- Larson, R. B. 2003, *Rep.Prog.Phys.*, 66, 1651
- Lee, M.-Y. et al., 2010, *ApJ*, in preparation
- Lucy, L. B. 1974, *AJ*, 79, 754
- Mei, S. et al., 2007, *ApJ*, 655, 144
- Nakanishi, H., Sofue, Y., & Koda, J. 2005, *PASJ*, 57, 905
- Rhee, M.-H. 1996, PhD Thesis, University of Groningen
- Rhee, M.-H., & Broeils, A. H. 2005, *JASS*, 22, 89
- Rhee, M.-H., & van Albada, T. S. 1996, *A&AS*, 115, 407
- Sakamoto, K. et al., 1999, *ApJS*, 124, 403
- Sandage, A., & Tammann, G. A. 2006, *ApJ*, submitted (astro-ph/0608677)
- Sofue, Y. et al., 2003, *PASJ*, 55, 17S
- Solomon, P. M., & Barrett, J. W. 1991, in *IAU Symp. 146, Dynamics of Galaxies and Their Molecular Cloud Distributions*, ed. F. Combes & F. Casoli (Dordrecht: Kluwer), 235
- van den Bergh, S. 1976, *ApJ*, 206, 883

- van der Hulst, J. M. et al., 1992, in ASP Conf. Ser. 25 Astronomical Data Analysis Software and System I, ed. D. M. Worall, C. Biemesderfer, & J. Barnes, 131
- van Gorkom, J. H. et al., 1984, in Groups and Clusters of Galaxies, ed. F. Mardirossian, G. Giuricin, & M. Mezzetti (Dordrecht: Reidel), 261
- Verheijen, M. A. W. 1997, PhD Thesis, University of Groningen
- Warmels, R. H. 1988, A&AS, 72, 427
- Yasuda, N. et al., 1997, ApJS, 108, 417
- Young, J. S. et al., 1989, ApJS, 70, 699
- Young, J. S., & Scoville, N. 1991, ARA&A, 29, 581
- Young, J. S. et al., 1995, ApJS, 98, 219
- Yun, M. S., Reddy, N. A., & Condon, J. J. 2001, ApJ, 554, 803